Science Translational Medicine
AAAS

stm.sciencemag.org/cgi/content/full/11/523/eaaw1565/DC1

Supplementary Materials for

Synthetic mRNA nanoparticle-mediated restoration of p53 tumor suppressor sensitizes *p53*-deficient cancers to mTOR inhibition

Na Kong, Wei Tao*, Xiang Ling, Junqing Wang, Yuling Xiao, Sanjun Shi, Xiaoyuan Ji, Aram Shajii, Silvia Tian Gan, Na Yoon Kim, Dan G. Duda, Tian Xie*, Omid C. Farokhzad*, Jinjun Shi*

*Corresponding author. Email: wtao@bwh.harvard.edu (W.T.); tianxie@hznu.edu.cn (T.X.); ofarokhzad@bwh.harvard.edu (O.C.F.); jshi@bwh.harvard.edu (J.S.)

Published 18 December 2019, *Sci. Transl. Med.* **11**, eaaw1565 (2019)
DOI: 10.1126/scitranslmed.aaw1565

This PDF file includes:

Materials and Methods

Materials

L-Cystine dimethyl ester dihydrochloride ($(H\text{-}Cys\text{-}OMe)_2 \cdot 2HCl$), trimethylamine, cationic ethylenediamine core-poly(amidoamine) (PAMAM) generation 0 dendrimer (G0), and fatty acid dichloride were obtained from Sigma-Aldrich. DMPE-PEG with PEG molecular weight (MW) 2000 and DSPE-PEG with PEG molecular weight (MW) 5000 were purchased from Avanti Polar Lipids. Lipofectamine 2000 (Lip2k) was purchased from Invitrogen. *EGFP*-mRNA (modified with 5-methylcytidine and pseudouridine) and CleanCap Cyanine 5 FLuc mRNA (control Cy5-labled *Luc*-mRNA) were purchased from TriLink Biotechnologies. Everolimus (RAD001) was obtained from Sigma-Aldrich. Primary antibodies used for western blot experiments and immunofluorescent and immunohistochemistry staining: anti-p53 (Santa Cruz Biotechnology, sc-126; 1:1,000 dilution), anti-BCL-2 (Abcam, ab59348; 1:1,000 dilution), anti-BAX (Cell Signaling Technology, #2774; 1:1,000 dilution), anti-PUMA (Santa Cruz Biotechnology, H-136; 1:1,000 dilution), anti-Cleaved Caspase3 (Cell Signaling Technology, #9661; 1:1,000 dilution), anti-Cleaved Caspase9 (Abcam, ab2324; 1:1,000 dilution), anti-p21(Abcam, ab109520; 1:2,000 dilution), anti-Cyclin E1 (Abcam, ab3927; 1:2,000 dilution), anti-mTOR (Cell Signaling Technology, #2972; 1:1,000 dilution), anti-p-mTOR (Cell Signaling Technology, #5536;1:1,000 dilution), anti-p-p70S6K (Cell Signaling Technology, #9205; 1:2,000 dilution), anti-p-4EBP1 (Cell Signaling Technology, #13443; 1:2,000 dilution), anti-LC3B (ABclonal, A7198; 1:1000 dilution), anti-SQSTM1/p62 (Abcam, ab56416;1:2,000 dilution), anti-mouse p53 (Santa Cruz Biotechnology, sc-393031; 1:1000 dilution), anti-p-AMPKα (Cell Signaling Technology, #2535S; 1:1000 dilution), anti-p-ACCα (Cell Signaling Technology, #11818S; 1:1000 dilution), anti-TIGAR (Abcam, ab37910; 1:1000 dilution), anti-BECLIN1 (Cell Signaling Technology, #3495; 1:2000 dilution), anti-CD31 (Servicebio, GB11063-3; 1:250 dilution). Anti-GAPDH (Cell Signaling Technology, #5174; 1:2,000 dilution), anti-beta-Actin (Cell Signaling Technology; 1: 2,000 dilution). Anti-rabbit and anti-mouse horseradish peroxidase (HRP)-conjugated secondary antibodies were obtained from Cell Signaling Technology. Secondary antibodies used for CLSM experiments included: Alexa Fluor 488 Goat-anti Rabbit IgG (Life Technologies, A-11034) and Alexa Fluor 647 Goat-anti Mouse IgG (Life Technologies, A-28181). The cationic lipid-like compound G0-C14 was prepared through a ring opening reaction of 1,2 epoxytetradecane with G0 according to previously described methods (*38*). The hydrophobic PDSA polymers were synthesized by one-step polycondensation of $(H\text{-}Cys\text{-}OMe)_2 \cdot 2HCl$ and the fatty acid dichloride as described (*41*), and characterized with the ^{1}HNMR spectra using a Mercury VX-300 spectrometer at 400 MHz.

Cell lines

The *p53*-null human hepatocellular carcinoma (HCC) cell line Hep3B (Hep 3B2.1-7, ATCC#HB-8064) and the *p53*-null human non-small cell lung cancer (NSCLC) cell line H1299 (ATCC#CRL-5803) were purchased from American Type Culture Collection (ATCC). The *p53*-null murine hepatocellular carcinoma cell line RIL-175 was obtained from Prof. Dan G. Duda's lab at Massachusetts General Hospital. Eagle's Minimum Essential Medium (EMEM; ATCC) was used to culture Hep3B cells, and Roswell Park Memorial Institute 1640 (RPMI-1640; ATCC) was used to maintain H1299 cells. Dulbecco's Modified Eagle's Medium (DMEM; ATCC) was used to culture RIL-175 cells. The cell culture medium was supplemented with 1% penicillin/streptomycin (Thermo-Fisher Scientific) and 10% fetal bovine serum (FBS; Gibco).

Synthesis of chemically modified *p53*-mRNA

The plasmid carrying the open-reading frame (ORF) of *p53* with a T7 promoter was purchased from Addgene. Linearized DNA was digested with endonuclease HindIII/ApaI. Then, *p53* ORF containing T7 promoter was amplified by PCR reaction and purified according to the manufacturer's protocol. For in vitro transcription (IVT), the MEGAscript T7 Transcription kit (Ambion) was used together with 1-2 μg purified PCR products (templates), 6 mM 3′-0-Me-m^{7}G(5′)ppp(5′)G (anti-reverse cap analog, ARCA), 1.5 mM GTP, 7.5 mM 5-methyl-CTP, 7.5 mM ATP, and 7.5 mM pseudo-UTP (TriLink Biotechnologies). Reactions were conducted at 37°C for 4 h and followed by DNase treatment. Afterwards, a poly(A) tailing kit (Ambion) was used for adding 3′ poly(A)-tails to IVT RNA transcripts. The *p53*-mRNA was purified by the MEGAclear kit (Ambion), followed by treatment with Antarctic Phosphatase (New England Biolab) at 37°C for 30 min. Large amounts of *p53*-mRNA were custom-synthesized by TriLink Biotechnologies with 100-150 μg template containing *p53* ORF and T7 promoter.

Electrostatic complexation between G0-C14 and mRNA

To evaluate the complexation of cationic compound G0-C14 with mRNA, we performed an electrophoresis study with E-Gel 2% agarose gels (Invitrogen) with naked *p53*-mRNA or *p53*-mRNA complexed with G0-C14 (weight ratios of G0-C14/mRNA: 0.1, 1, 5, 10, 15, and 20). To assess the stability of mRNA in organic solvent (DMF), naked mRNA was incubated with DMF for 30 min and then loaded into agarose gels. The gel was imaged under UV light, and the bands from all groups were analyzed.

Formulation of the lipid-polymer hybrid mRNA NPs. A modified self-assembly method was adopted to prepare the mRNA-encapsulated lipid-polymer hybrid NPs. This method included the following steps: G0-C14, PDSA, and lipid-PEGs were dissolved separately in DMF to form a homogeneous solution at concentrations of 2.5 mg/ml, 20 mg/ml, and 20 mg/ml, respectively. 24 μg of mRNA (in 24 μl of water) and 360 μg of G0-C14 (in 144 μl of DMF) were mixed gently (at a G0-C14/mRNA weight ratio of 15) to enable the electrostatic complexation. Afterwards, 4 mg of PDSA polymers (in 200 μl of DMF) and 2.8 mg of hybrid lipid-PEGs (in 140 μl of DMF) were added to the mixture successively and further mixed together. The final mixture was added dropwise to 10 ml of DNase/RNase-free HyClone HyPure water (Molecular Biology Grade) under magnetic stirring (800 rpm) for 30 min. An ultrafiltration device (EMD Millipore, MWCO 100 kDa) was used to remove the organic solvent and free compounds in the formed NP dispersion via centrifugation. After washing 3 times with HyPure water, the mRNA NPs were collected and dispersed in pH 7.4 PBS buffer for further use or stored at -80 °C. We prepared the engineered mRNA NPs with three different DSPE-PEG/DMPE-PEG ratios (NP_{25}: 25% of DSPE-PEG in lipid-PEG layer; NP_{50}: 50% of DSPE-PEG in lipid-PEG layer; NP_{75}: 75% of DSPE-PEG in lipid-PEG layer; w/w%). Two Cy5-labelled mRNAs with different molecular properties (*EGFP*-mRNA with a length of 996 nucleotides and *Luc*-mRNA with a length of 1,921 nucleotides) were chosen as model mRNAs to verify their potential effects on encapsulation and NP properties. As shown in **fig. S6**, different compositions of G0-C14/PDSA/lipid-PEG (**table S1**) changed NP size. Nevertheless, although the mRNA length of *Luc*-mRNA is ~2-fold longer than that of *EGFP*-mRNA, its effect on NP size was not drastic. In addition, there was no obvious difference in mRNA encapsulation efficiency between the *EGFP*-mRNA NPs and the *Luc*-mRNA NPs for each formulation (**fig. S7**). Considering the NP properties (especially the NP size) and the transfection efficacy (**fig. S8**), we used 25% of DSPE-PEG (w/w%) in lipid-PEG layer (0.7 mg of DSPE-PEG and 2.1 mg of DMPE-PEG in 2.8 mg of hybrid lipid-PEGs; NP_{25}) for all in vitro studies.

Characterization of the synthetic mRNA NPs

We used dynamic light scattering (DLS, Brookhaven Instruments Corporation) to determine the size of the engineered mRNA NPs and their stability in PBS (containing 10% serum) at 37 °C over a span of 72 h. JEOL 1200EX-80kV transmission electron microscope (TEM) was used to visualize the morphology of mRNA NPs. To test the mRNA encapsulation efficiency (EE%), Cy5-mRNA NPs were prepared according to the aforementioned method. In brief, 100 μl of dimethyl sulfoxide (DMSO) was used to treat 5 μl of the NP solution, and fluorescence intensity of Cy5-mRNA was tested by a Synergy HT multi-mode microplate reader. The amount of loaded mRNA in the engineered NPs was calculated to be ~50% in this study.

Evaluation of the redox-responsive property of the mRNA NPs

The prepared Cy5-mRNA NPs were suspended in 1 ml of PBS (pH 7.4) containing DTT at the concentration of 10 mM. The morphology of the NPs was visualized by TEM after 2 or 4 hours of incubation. In addition, to verify the influence of redox on the mRNA release, Cy5-mRNA NPs were suspended in 1 ml of PBS and added in a Float-a-lyzer G2 dialysis device (MWCO = 100 kDa, Spectrum), which was immersed in PBS or PBS containing DTT at different concentrations (1 mM and 10 mM) at 37 °C. At different time points (1, 2, 4, 8, 12, and 24 h), 5 μl of the NP solution was taken and mixed with 100 μl of DMSO. The fluorescence intensity of Cy5-mRNA was tested by a microplate reader.

Cell viability and transfection efficiency of *EGFP*-mRNA NPs

The *p53*-null Hep3B cells or H1299 cells were plated in 96-well plates at a density of 3×10^3 cells per well. After 24 hours of cell adherence, cells were transfected with *EGFP*-mRNA at various mRNA concentrations (0.102, 0.207, 0.415, or 0.830 μg/ml) for 24 hours, followed by the addition of 0.1 ml fresh complete medium and further incubation for another 24 hours to evaluate cell viability as well as the transfection efficiency. Lip2k was used as a positive control for transfection efficiency comparison with the NPs. Cell viability was tested by AlamarBlue assay, which is a non-toxic assay that can continuously check real-time cell proliferation through a microplate reader (TECAN, Infinite M200 Pro). Absorbance was examined by a 96-well SpectraMax plate reader (Molecular Devices) at 545 nm and 590 nm. To measure the transection efficiency, cells were treated with *EGFP*-mRNA by NPs or Lip2k for 24 hours, detached with 2.5% EDTA trypsin, and collected in PBS solution, followed by evaluating GFP expression using flow cytometry (BD Biosystems). The percentages of EGFP-positive cells were calculated and analyzed by Flowjo software.

In vitro cell viability of *p53*-mRNA NPs or their combination with everolimus

The *p53*-null Hep3B or H1299 cells were plated in a 96-well plate at a density of 5×10^3 cells per well. After 24 hours of cell adherence, cells were transfected with *EGFP*-mRNA NPs (control NPs), *p53*-mRNA NPs, everolimus, or *p53*-mRNA NPs together with everolimus. The concentration of mRNA used was 0.415 μg/ml, whereas the concentration of everolimus was 32 nM in Hep3B cells or 16 nM in H1299 cells. After 24 hours of incubation followed by addition of 0.1 ml fresh complete medium for another 24 hours, the AlamarBlue cell viability assay mentioned above was used to verify the in vitro efficacy of *p53*-mRNA NPs and their ability to sensitize cells to everolimus.

Colony formation assay

The cells' proliferation ability was measured by a soft agar colony formation assay. Cells were treated with *p53*-mRNA NPs or empty NPs for 48 hours. Then, cells were suspended in 0.36% agarose

(Invitrogen) diluted in the complete medium, then reseeded into 6-well plates at low density (~1000 cells per well) containing a 0.75% preformed layer of agarose and incubated for 2 weeks. The plates were then washed with PBS and fixed in 4% paraformaldehyde for 20 min and then stained with 0.005% crystal violet. The images of all the wells were scanned and analyzed.

Apoptosis and cell cycle detection in vitro

We used an FITC Annexin V/Propidium iodide (PI) apoptosis detection kit (BD Biosciences) to detect apoptosis. In brief, 1×10^6 cells were seeded into 6-well plates. After attachment overnight, cells were treated with *p53*-mRNA NPs for 24 hours before being mixed with 1 ml fresh medium and continuing to culture for another 24 h. All the attached cells together with the floating cells in the medium were harvested, washed with PBS twice, and dispersed in 1× binding buffer solution (ice-cold) at a concentration of 1×10^6 cells/ml. 5 μl of FITC Annexin V and 5 μl of PI were further mixed with 100 μl of the cell suspension. We then incubated the mixture at room temperature for 15 min in a dark environment and performed analysis using the FACS Calibur Flow Cytometer (BD Biosystems). Cells were incubated for 48 hours with empty NPs, naked *p53*-mRNA, or *p53*-mRNA NPs washed in PBS and fixed with 70% ethanol overnight, then washed in PBS twice and incubated with PI for 30 minutes at 37°C; cell-cycle fractions (percentage of cells with fractional DNA content in G1, S, and G2/M phases of the cycle) were estimated by flow cytometry and analyzed by Flowjo software.

Western blot assay

Cells or dissected tumors in each group were lysed in a lysis buffer (1 mM EDTA, 20 mM Tris-HCl pH 7.6, 140 mM NaCl, 1% aprotinin, 1% NP-40, 1 mM phenylmethylsulphonyl fluoride, and 1 mM sodium vanadate), and supplemented with protease inhibitor cocktail (Cell Signaling Technology). Protein concentration was detected by a bicinchoninic acid (BCA) Protein Assay Kit (Pierce). 25 μg of proteins were loaded on 6-12% precast gels (Invitrogen), and then transferred to Immobilon PVDF membranes (Bio-Rad, 162-0176 and 162-0177). The transferred membranes were blocked with 5% bovine serum albumin (BSA) in TBST (150 mM NaCl, 50 mM Tris-HCl at pH 7.4, and 0.1% Tween 20) for 1 hour at room temperature, and were further incubated with primary antibodies overnight at 4°C. The immunoreactive bands were detected with appropriate HRP-conjugated secondary antibodies. Band density was detected by enhanced chemiluminescence (ECL) detection system (Amersham/GE Healthcare).

Gene expression via quantitative real time polymerase chain reaction (qRT-PCR)

qRT-PCR was used to quantify the expression of autophagy-related genes (*DRAM1, ISG20L1, ULK1, ATG7, BECN1, ATG12,* and *SESN1*) and p53 target gene *TIGAR* in Hep3B and H1299 cell lines. Total RNA was isolated using TRIzol (Invitrogen Life Technology) according to the protocol. RNA was quantitated by UV absorbance at 260 nm. cDNA was reverse-transcribed (RT) using a complementary DNA synthesis kit (Thermo Fisher Scientific, SuperScript III First-Strand Synthesis System). The qRT-PCR was performed in Real-Time PCR Detection instrument (Qiagen, Rotor Gene Q Series) using SYBR Green dye (Qiagen, Rotor-Gene SYBR Green PCR Kit). 25 μl of mixture containing 100 ng cDNA, 1 μM primer dilution, and 12.5 μl 2×Roter-Gene SYBR Green PCR Master Mix was used in each PCR reaction. Fluorescence signal was recorded at the endpoint of each cycle during the 40 cycles (denaturizing 15 sec at 95 °C, annealing 45 sec at 60 °C, and extension 20 sec at 72 °C). *GAPDH* was used as internal control gene for normalization. Relative gene expression was calculated by the comparative threshold cycle (CT), which represents the inverse of the amount of mRNA in the initial sample.

Design of the primers for qRT-PCR

Primers were designed via National Center for Biotechnology Information website: https://www.ncbi.nlm.nih.gov/tools/primer-blast/. Primers were selected according to following criteria: (1) length between 18 and 24 bases; (2) melting temperature (Tm) between 57 °C and 60 °C (optimal Tm 58 °C); and (3) G+C content between 40% and 60% (optimal 50%). Primer sequences are listed in **table S2**.

Immunofluorescent staining and TEM detection

Cells or tumor tissues were fixed with 4% paraformaldehyde (Electron Microscopy Sciences) at room temperature for 15 min, followed by permeabilization in 0.2% Triton X-100-PBS for 10 min. Samples were further incubated with PBS blocking buffer (containing 2% BSA, 2% normal goat serum, and 0.2% gelatin) at room temperature for 30 min. Afterwards, the samples were incubated with primary antibody overnight at 4°C, washed with PBS, and incubated in goat anti-rat-Alexa Fluor 647 (Molecular Probes) in blocking buffer (1:1000 dilution) at room temperature for 60 min. Stained samples were washed with PBS, nuclei were stained using Hoechst 33342 (Molecular Probes-Invitrogen, H1399, 1:2000 dilution in PBS), and the samples were mounted on slides with Prolong Gold antifade mounting medium (Life Technologies). For TEM detection, treated cells were washed and fixed by 2.5% glutaraldehyde solution (Sigma-Aldrich, G5882) overnight. After treatment with 1.5% osmium tetroxide, the samples were dehydrated in graded ethanol, and then embedded in 812 resin (Ted Pella, 18109). Thin sections were sliced and poststained with 2% uranyl acetate, then imaged with the TECNAI 10 TEM (Philips).

Quantification of GFP-LC3B puncta

For GFP-LC3B autophagy assays, prepackaged viral particles expressing recombinant GFP-LC3B (LentiBrite GFP-LC3B Lentiviral Biosensor; Millipore, 17-10193) were used to generate GFP-LC3B stable cell lines. Then, GFP-LC3B stable cells were treated with everolimus or *p53*-mRNA NPs and incubated for 24 hours at 37^{o}C. A confocal fluorescence microscope was used to observe the fluorescence of GFP-LC3B. To quantify the extent of autophagy, cells showing accumulation of GFP-LC3B in vacuoles or dots were counted. Cells showing several intense punctate GFP-LC3B aggregates but no nuclear GFP-LC3B were defined as autophagic, whereas those presenting diffuse distributions of GFP-LC3B positive puncta (green) in both the cytoplasm and nucleus were considered as non-autophagic.

Immunohistochemistry (IHC) staining

Samples were obtained from different tumor models (*p53*-null Hep3B liver xenograft tumor model and liver metastases of *p53*-null H1299 lung tumor model). Sections were fixed in 4% buffered formaldehyde solution for 24 hours and embedded in paraffin, then sectioned into thin slices (5 μm thick) to be further deparaffinized, rehydrated in a graded ethanol series, and washed in distilled water. To retrieve the antigen, tumor tissue sections were incubated in 10 mM citrate buffer (pH=6) for 30 min, washed in PBS, and immersed in 0.3% hydrogen peroxide (H_2O_2) for 20 min, then incubated in blocking buffer (5% normal goat serum and 1% BSA) for 60 min. Tissue sections were then incubated with primary antibodies (PBS solution supplemented with 0.3% Triton X-100) at 4°C overnight in a humid chamber. After being rinsed with PBS, the samples were incubated with biotinylated secondary antibody at room temperature for 30 min, washed again with PBS, followed by incubation with the avidin–biotin–horseradish peroxidase complex (ABC kit, Vector Laboratories, Inc). After being washed again, stains were processed with the diaminobenzidine peroxidase substrate kit (Impact DAB, Vector Laboratories,

Inc) for 3 min. Sections were evaluated under a Leica Microsystem microscope after being counterstained with hematoxylin (Sigma), dehydrated, and mounted.

TUNEL apoptosis assay

Apoptotic cells in tumor tissues were measured by TUNEL staining using a detection kit (*In Situ* Cell Death Detection Kit, TMR red; Roche, #12-156-792-910) according to the manufacturer's protocol. Tumor sections were extracted and fixed in formalin, embedded in paraffin, and sectioned at a thickness of 5 μm. DAPI stain was used to assess total cell number. TUNEL-positive cells had a pyknotic nucleus with red fluorescent staining, representative of apoptosis. Images of the sections were taken by a fluorescence microscope (Olympus).

Combination index (*CI*) calculation

A reported method was used to calculate the *CI* value (*51*, *52*). Briefly, the expected value of combination effect (*Vexp*) between treatment of everolimus and *p53*-mRNA NPs was calculated using formula (1) as follows:

$$Vexp = (\frac{V1}{Vctrl}) \times (\frac{V2}{Vctrl}) \times Vctrl \quad (1)$$

where *Vctrl* is the observed value of control group (cell viability for in vitro studies and tumor volume for in vivo studies), *V1* is the observed value of everolimus treatment, and *V2* is the observed value of *p53*-mRNA NPs treatment. The *CI* was then calculated using formula (2) as follows:

$$CI = \frac{Vexp}{Vobs} \quad (2)$$

where *Vobs* is the observed value of combination effect between treatments with everolimus and *p53*-mRNA NPs. The combination effect was evaluated by the value of *CI*, with $CI > 1$ indicating a synergistic effect.

SUPPLEMENTARY FIGURES

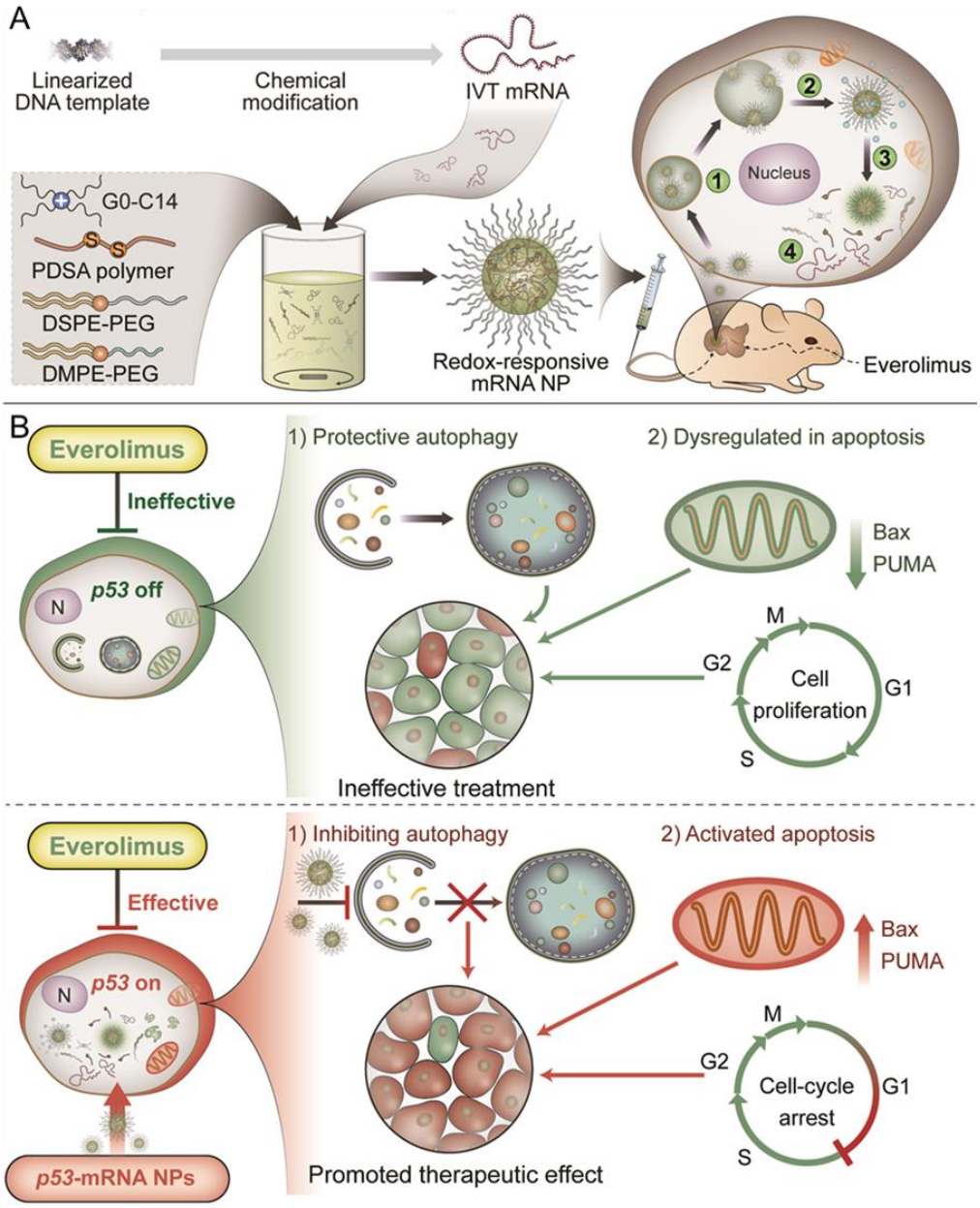

Fig. S1. Study summary. (**A**) Schematic representation of the synthesis of chemically modified mRNA and the formulation of redox-responsive lipid-polymer hybrid NPs for mRNA delivery. After intravenous injection, the synthetic mRNA NPs enter tumor tissues through the enhanced permeability and retention (EPR) effect for targeting tumor cells, followed by (1) NP endocytosis; (2) endosomal escape; and (3) redox-responsive release of (4) mRNA from the NPs. The released mRNA can then induce restoration of tumor suppressor proteins such as p53. (**B**) Schematic representation of the mechanism of *p53*-mRNA NP-mediated sensitization of cells to everolimus by inhibiting the activation of protective autophagy in *p53*-deficient cancer cells. Along with p53 restoration-induced apoptosis and cell cycle arrest, the combination of *p53*-mRNA NPs with everolimus is expected to show synergistic anti-tumor effect.

Fig. S2. The structure schematic of synthetic mRNA. It includes an anti-reverse cap analog (ARCA), untranslated regions (UTRs), an open reading frame (ORF), and a poly-A tail.

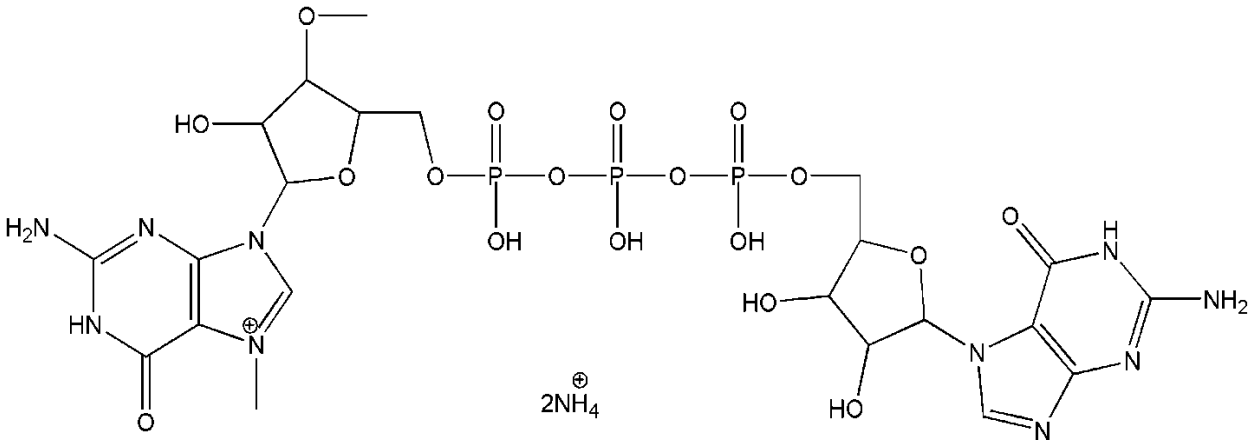

Fig. S3. The chemical structure of 3′-O-Me-m^{7}G(5′)ppp(5′)G ARCA cap.

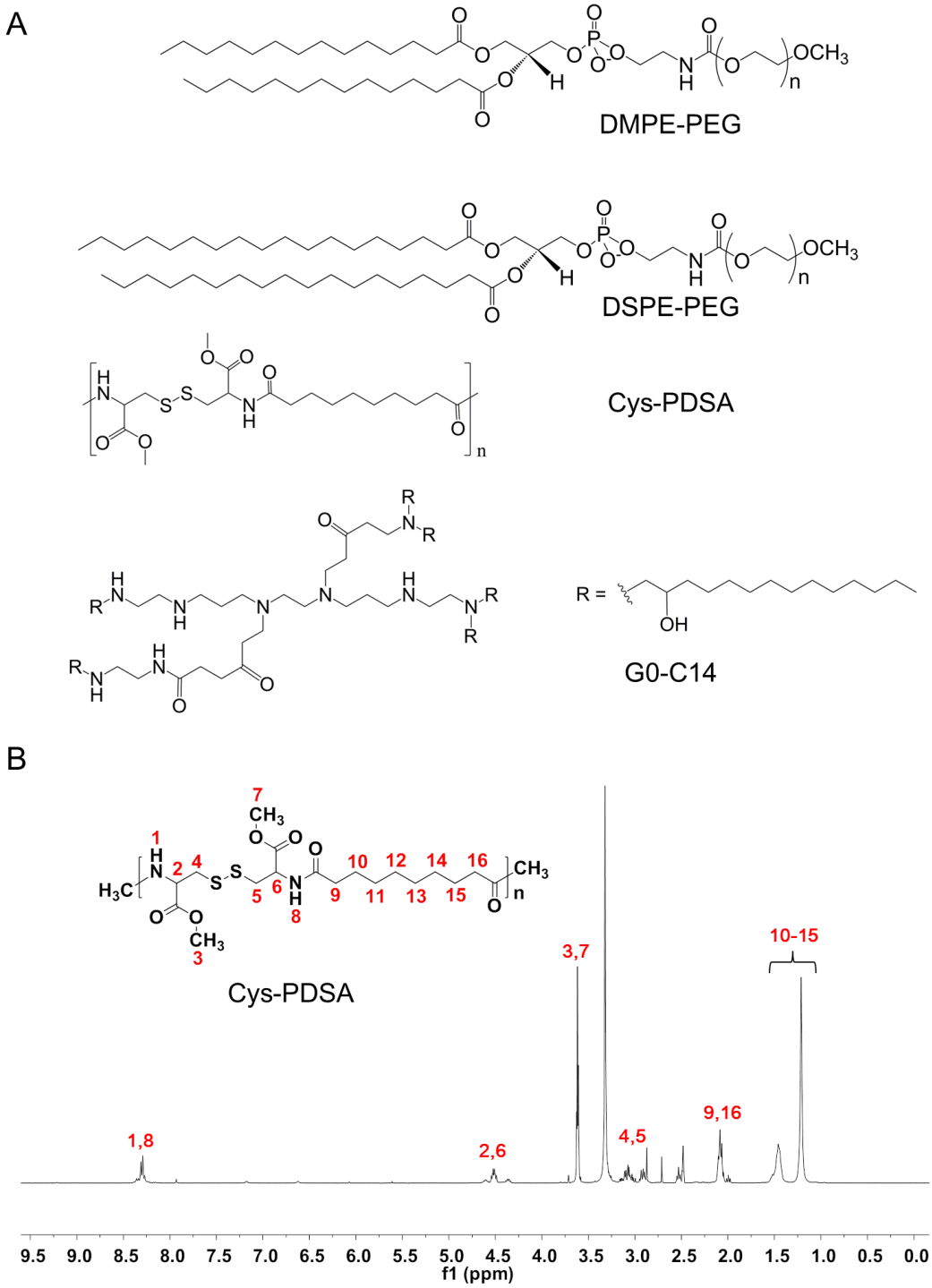

Fig. S4. Chemicals for NP synthesis. (**A**) Chemical structures of the lipid-PEGs (DMPE-PEG and DSPE-PEG), polymer (PDSA), and cationic lipid-like material (G0-C14). (**B**) ^{1}H NMR spectrum of the synthesized redox-responsive polymer PDSA.

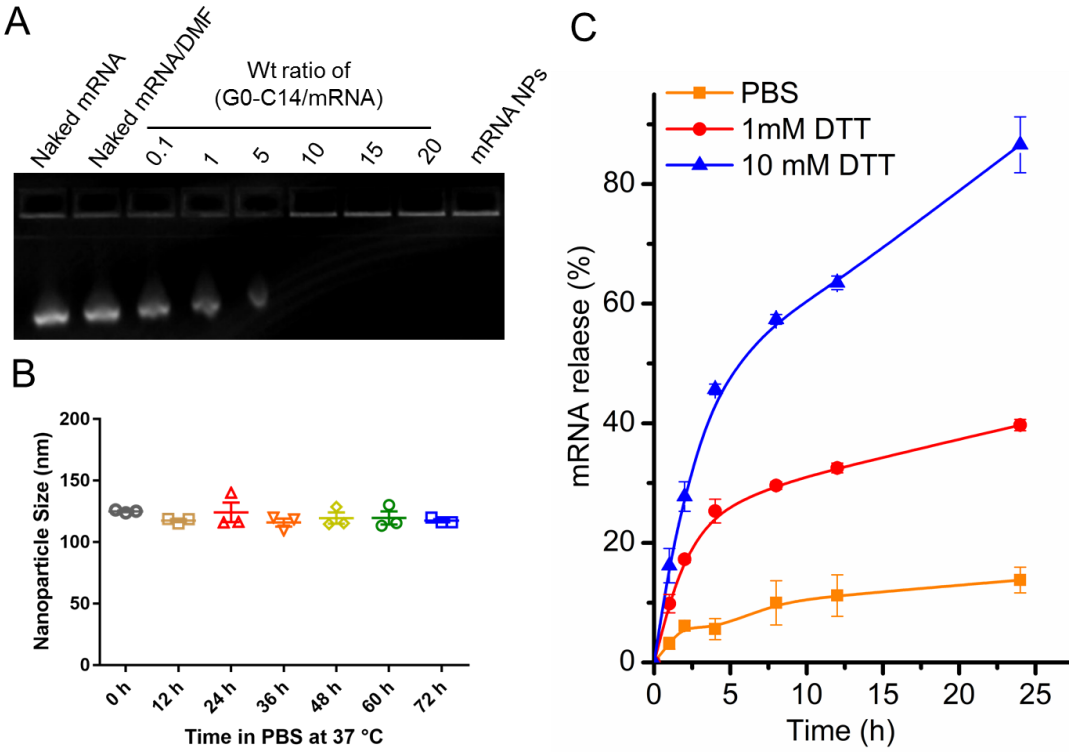

Fig. S5. Characterization of the engineered hybrid mRNA NPs. (**A**) Agarose gel electrophoresis assay of mRNA in nuclease-free water, DMF, or complexed with cationic G0-C14 at various weight ratios. The engineered mRNA NPs were also subjected to gel electrophoresis for detecting any mRNA leaching. (**B**) Stability of the engineered mRNA NPs over 3 days in PBS containing 10% serum at 37 °C. (**C**) In vitro release of Cy5-labeled mRNA from the engineered NPs in PBS, 1 mM DTT, and 10 mM DTT at 37 °C. Data shown as means ± S.E.M. (n=3).

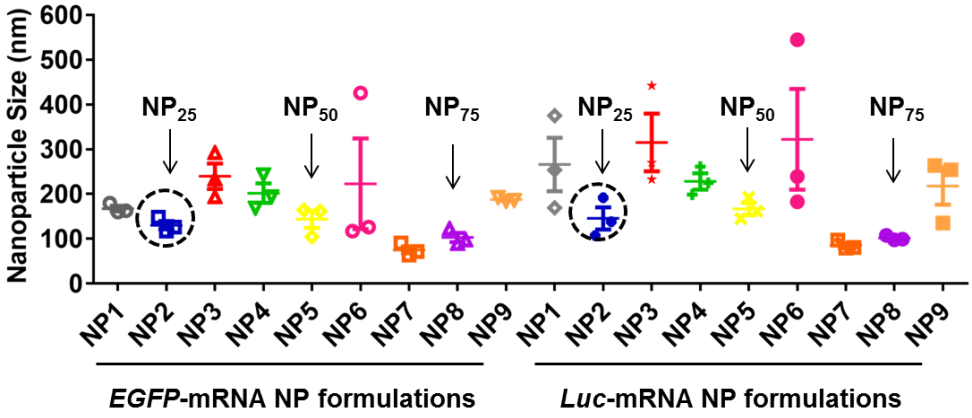

Fig. S6. Size of *EGFP*-mRNA NPs and *Luc*-mRNA NPs with various formulations. NP formulations with different ratios of composition are listed in table S1. Data shown as means ± S.E.M. (n=3).

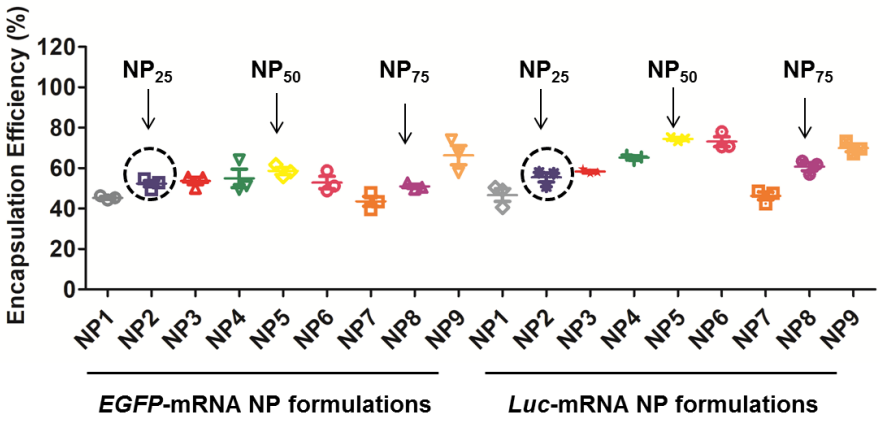

Fig. S7. Encapsulation efficiency of *EGFP*-mRNA NPs and *Luc*-mRNA NPs with various formulations. NP formulations with different ratios of composition are listed in table S1. Data shown as means ± S.E.M. (n=3).

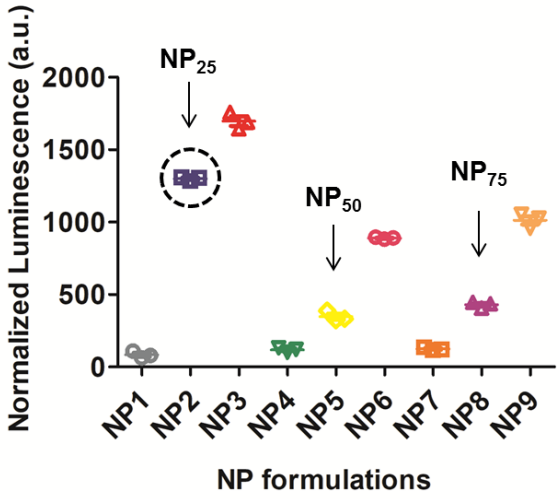

Fig. S8. Normalized luminescence intensity of Hep3B cells after treatment with various *Luc*-mRNA NP formulations at the mRNA dose of 0.830 μg/ml. NP formulations with different ratios of composition are listed in table S1. Data shown as means ± S.E.M. (n=3).

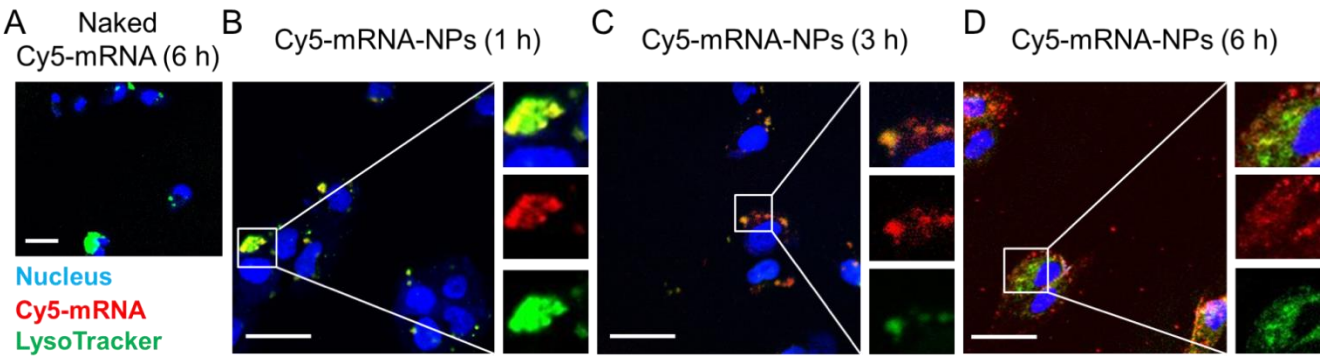

Fig. S9. Endosomal escape of mRNA NPs. Confocal laser scanning microscopy (CLSM) images of *p53*-null H1299 NSCLC cells after incubation with (**A**) naked Cy5-labeled mRNA (red) for 6 h, and (**B-D**) Cy5-labeled mRNA NPs for (**B**) 1 h, (**C**) 3 h, and (**D**) 6 h. Endosomes were stained by Lysotracker Green (green) and nuclei were stained by DAPI (blue). Scale bar, 50 μm.

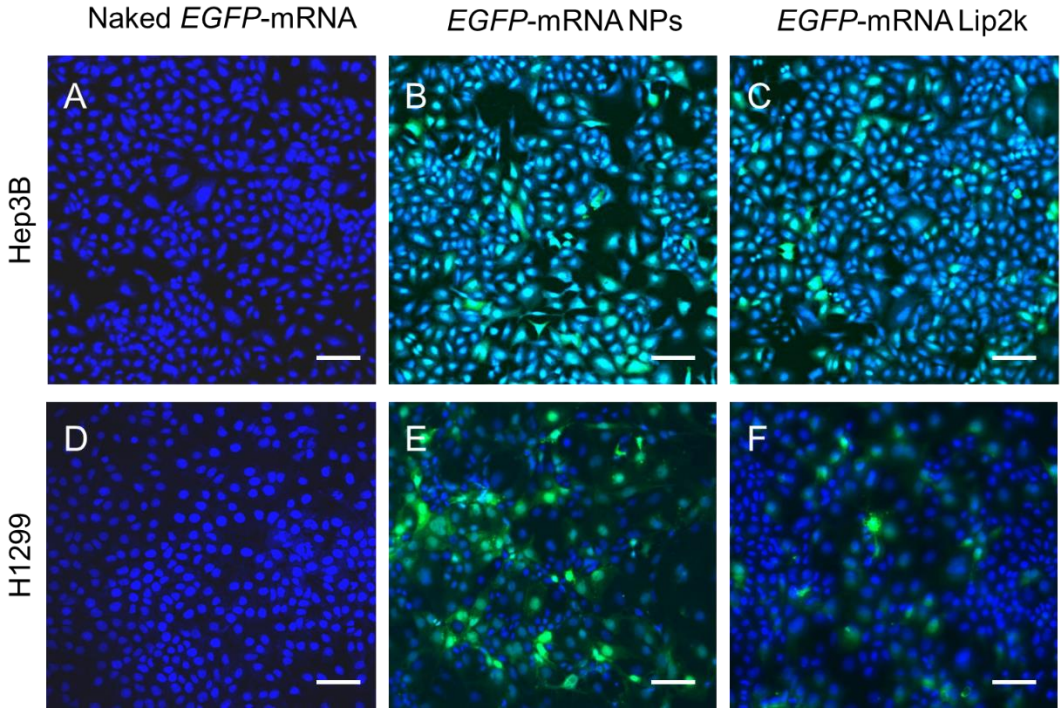

Fig. S10. Transfection efficacy verified by CLSM imaging. CLSM images of *p53*-null Hep3B cells transfected with (**A**) naked *EGFP*-mRNA, (**B**) *EGFP*-mRNA NPs, and (**C**) *EGFP*-mRNA Lip2k; and *p53*-null H1299 cells transfected with (**D**) naked *EGFP* mRNA, (**E**) *EGFP*-mRNA NPs, and (**F**) *EGFP*-mRNA Lip2k (scale bar, 100 μm).

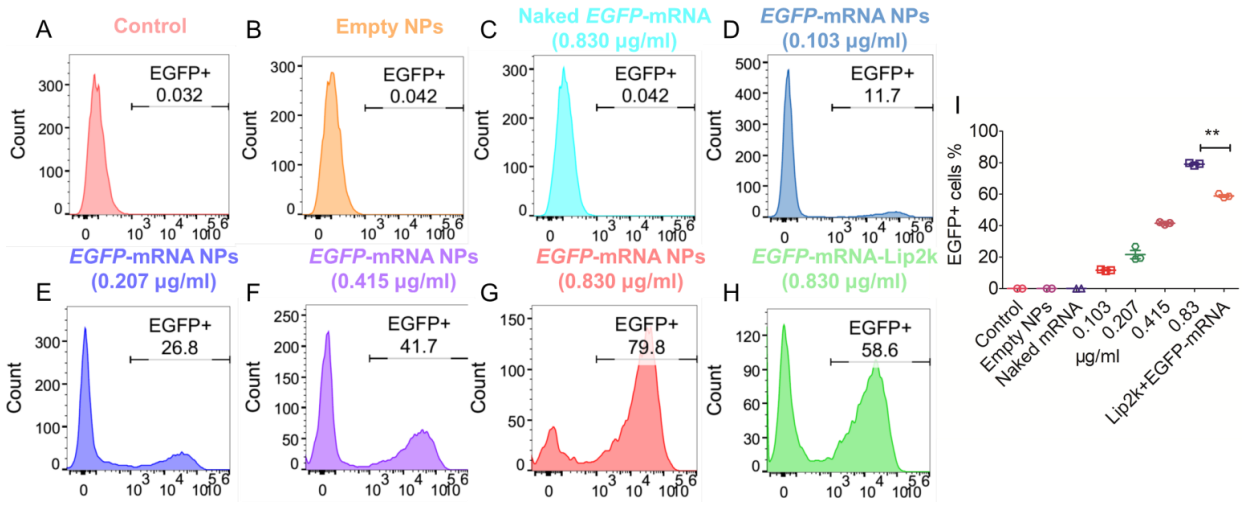

Fig. S11. Transfection efficacy verified by flow cytometry. Histogram analysis of the in vitro transfection efficiency in the *p53*-null H1299 NSCLC cells treated with (**A**) PBS, (**B**) empty NPs, (**C**) naked *EGFP*-mRNA (0.830 μg/ml), (**D**) *EGFP*-mRNA NPs (0.103 μg/ml), (**E**) *EGFP*-mRNA NPs (0.207 μg/ml), (**F**) *EGFP*-mRNA NPs (0.415 μg/ml), (**G**) *EGFP*-mRNA NPs (0.830 μg/ml), and (**H**) *EGFP*-mRNA Lip2k (0.830 μg/ml) by Flowjo software. (**I**) In vitro transfection efficiency (%EGFP positive cells) was determined by flow cytometry. Data shown as means ± S.E.M. (n=3), and statistical significance was determined using two-tailed t test (**P< 0.01).

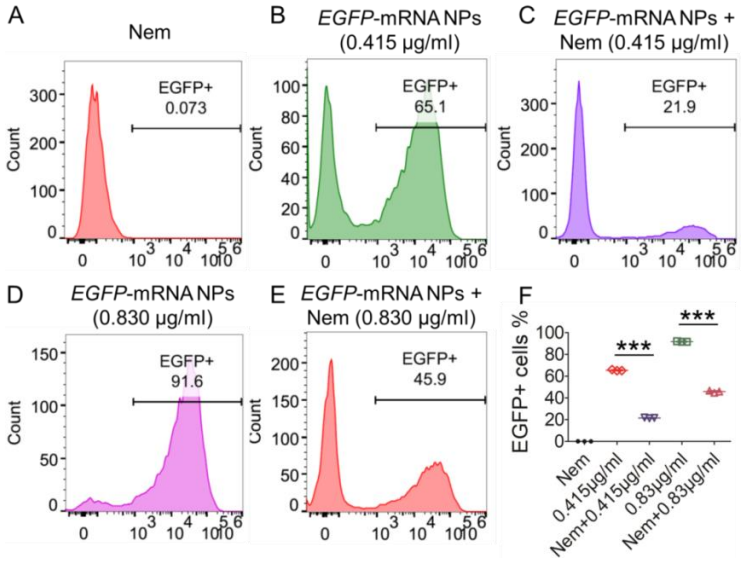

Fig. S12. Transfection efficacy after quenching intracellular GSH. Histogram analysis of the in vitro transfection efficiency in the *p53*-null Hep3B cells treated with (**A**) Nem (50 μM), (**B**) *EGFP*-mRNA NPs (0.415 μg/ml), (**C**) Nem (50 μM) for 1 h followed by the *EGFP*-mRNA NPs (0.415 μg/ml), (**D**) *EGFP*-mRNA NPs (0.830 μg/ml), and (**E**) Nem (50 μM) for 1 h followed by the *EGFP*-mRNA NPs (0.830 μg/ml). (**F**) In vitro transfection efficiency (%EGFP positive cells) was determined by flow cytometry. Data shown as means ± S.E.M. (n=3), and statistical significance was determined using two-tailed t test (***P< 0.001).

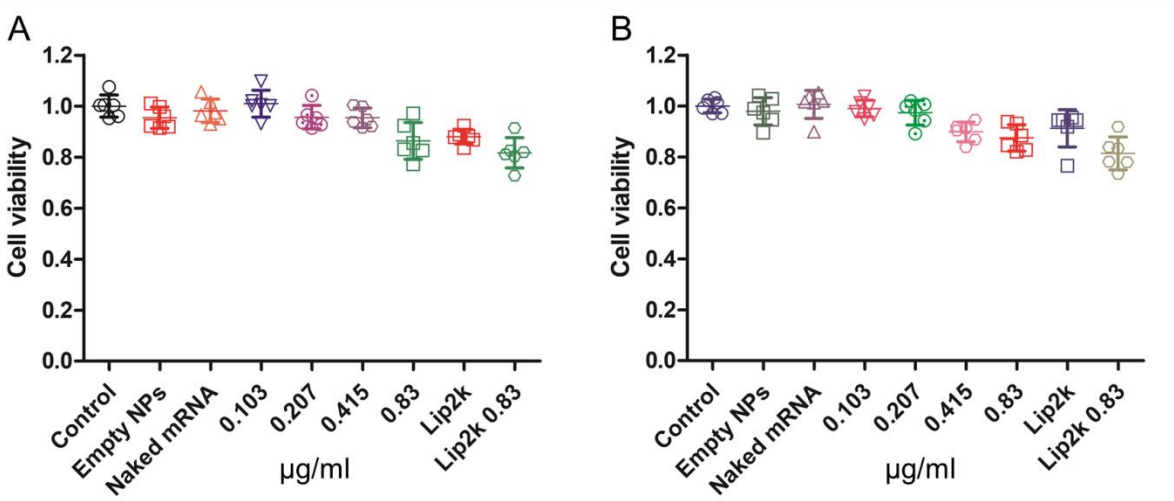

Fig. S13. In vitro toxicity of the synthetic *EGFP*-mRNA NPs. The viability of the (**A**) *p53*-null Hep3B cells and (**B**) *p53*-null H1299 cells after treatment with PBS, empty NPs, naked *EGFP*-mRNA (0.830 µg/ml), *EGFP*-mRNA NPs (0.103, 0.207, 0.415, or 0.830 µg/ml), or *EGFP*-mRNA Lip2k (0.830 µg/ml), as measured by AlamarBlue assay.

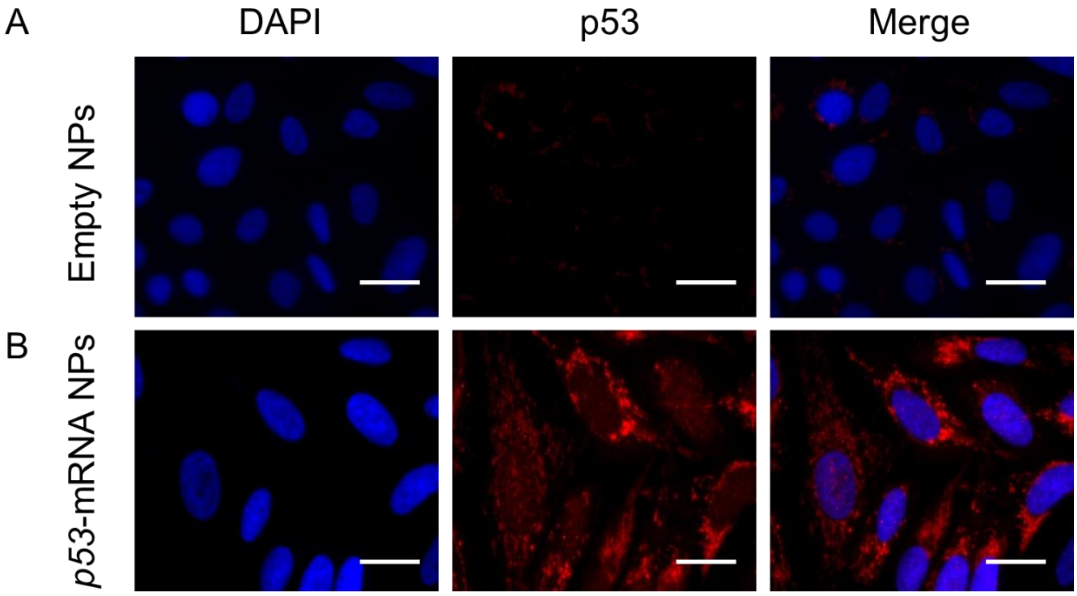

Fig. S14. IF staining of p53 in *p53*-null H1299 cells. Cells were treated with (**A**) empty NPs or (**B**) *p53*-mRNA NPs (scale bars, 25 µm).

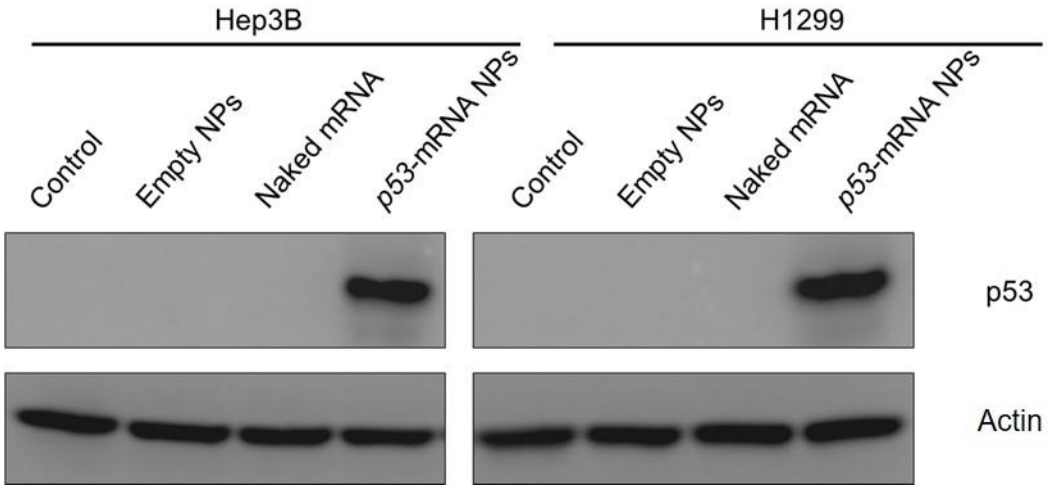

Fig. S15. WB analysis of p53 protein expression. Both *p53*-null Hep3B cells and *p53*-null H1299 cells were treated with PBS, empty NPs, naked *p53*-mRNA, or *p53*-mRNA NPs. Actin was measured as the loading control.

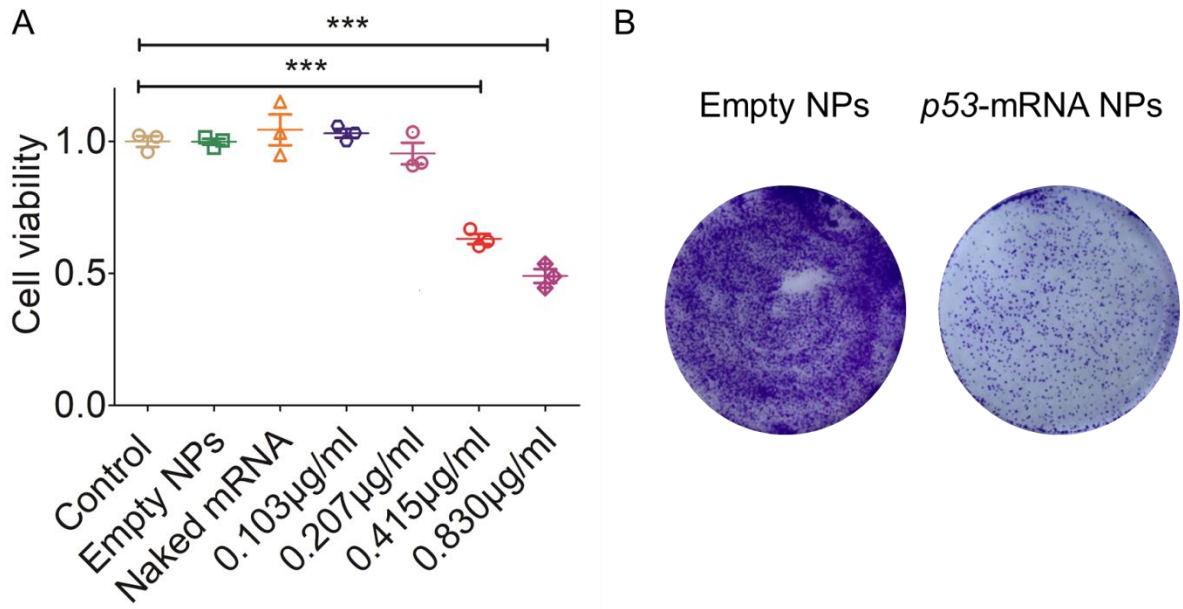

Fig. S16. In vitro therapeutic efficacy of the synthetic *p53*-mRNA NPs in *p53*-null H1299 cells. (**A**) The viability of H1299 cells after treatment with PBS, empty NPs, naked *p53*-mRNA (0.830 μg/ml), or *p53*-mRNA NPs (0.103, 0.207, 0.415, or 0.830 μg/ml), as measured by AlamarBlue assay. Statistical significance was determined by two-tailed t test (***P< 0.001). (**B**) Colony formation of H1299 cells after treatment with empty NPs vs. *p53*-mRNA NPs in 6-well plates.

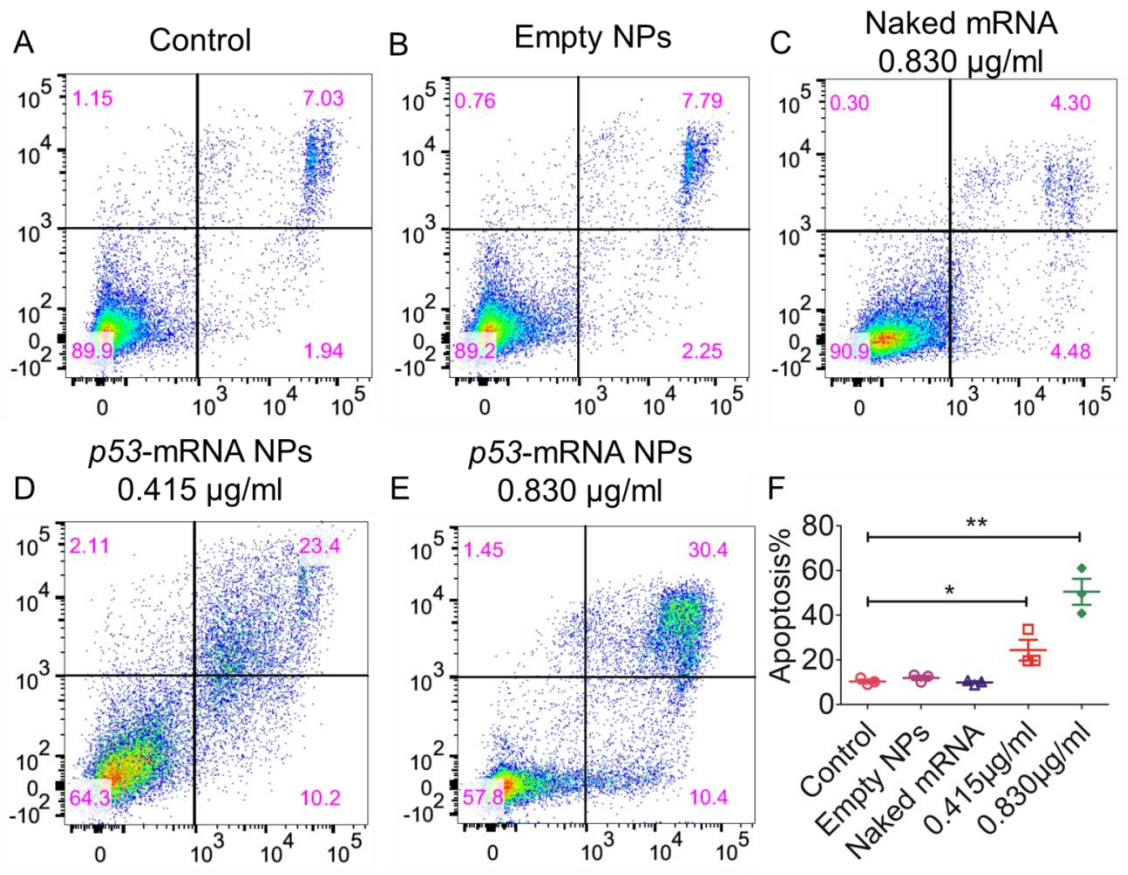

Fig. S17. Apoptosis of *p53*-null H1299 cells as determined by flow cytometry after different treatments. Cells were treated with (**A**) PBS, (**B**) empty NPs, (**C**) naked *p53*-mRNA (0.830 μg/ml), (**D**) *p53*-mRNA NPs (0.415 μg/ml), and (**E**) *p53*-mRNA NPs (0.830 μg/ml). (**F**) Histogram analysis of apoptosis in the respective groups by Flowjo software. Data shown as means ± S.E.M. (n=3), and statistical significance was determined using two-tailed t test (*P< 0.05, **P< 0.01).

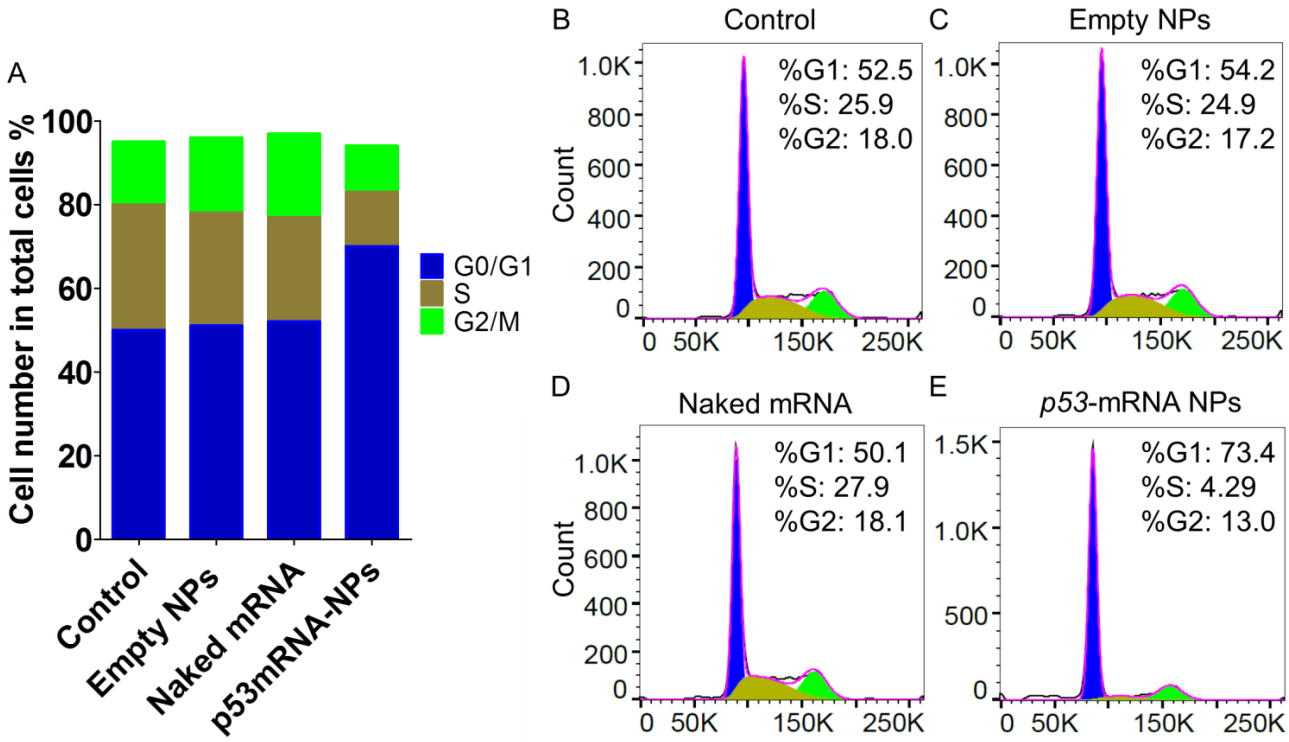

Fig. S18. G_1-phase cell cycle arrest induced by *p53*-mRNA NPs. (**A**) Cell cycle distributions of the *p53*-null H1299 cells after treatment with PBS, empty NPs, naked *p53*-mRNA, or *p53*-mRNA NPs. (**B-D**) Analysis of cell percentages in each cell cycle phase after treatment with (**B**) PBS, (**C**) empty NPs, (**D**) naked *p53*-mRNA, and (**E**) *p53*-mRNA NPs.

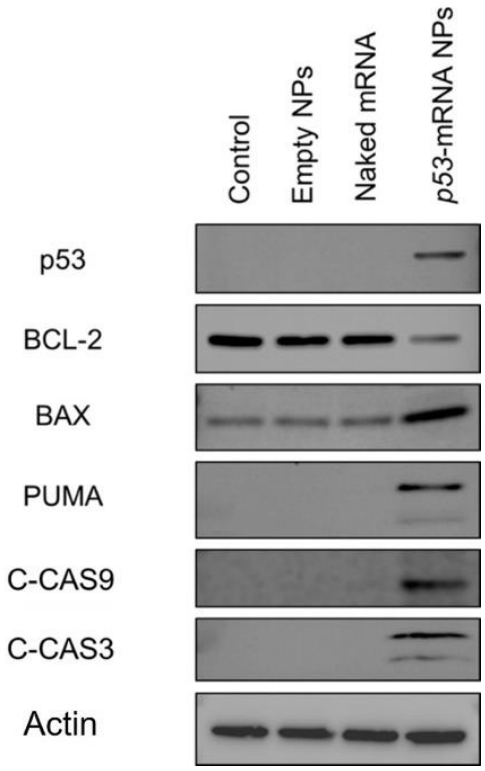

Fig. S19. WB analysis of apoptotic signaling pathway in *p53*-null H1299 cells after different treatments. Cells were treated with PBS, empty NPs, naked *p53*-mRNA, or *p53*-mRNA NPs. p53, BCL-2, BAX, PUMA, cleaved caspase9 (C-CAS9), and cleaved caspase3 (C-CAS3) proteins were detected. Actin was used as the loading control.

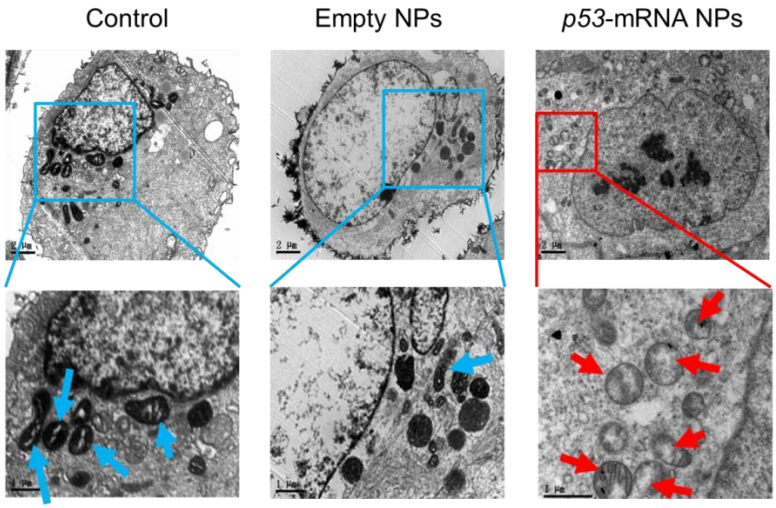

Fig. S20. TEM images of mitochondrial morphology in *p53*-null H1299 cells after different treatments. Images were obtained from control, empty NPs, and *p53*-mRNA NPs groups (blue arrow: normal mitochondria; red arrow: swelling mitochondria; scale bars in the raw images: 2 μm; scale bars in the enlarged images: 1 μm).

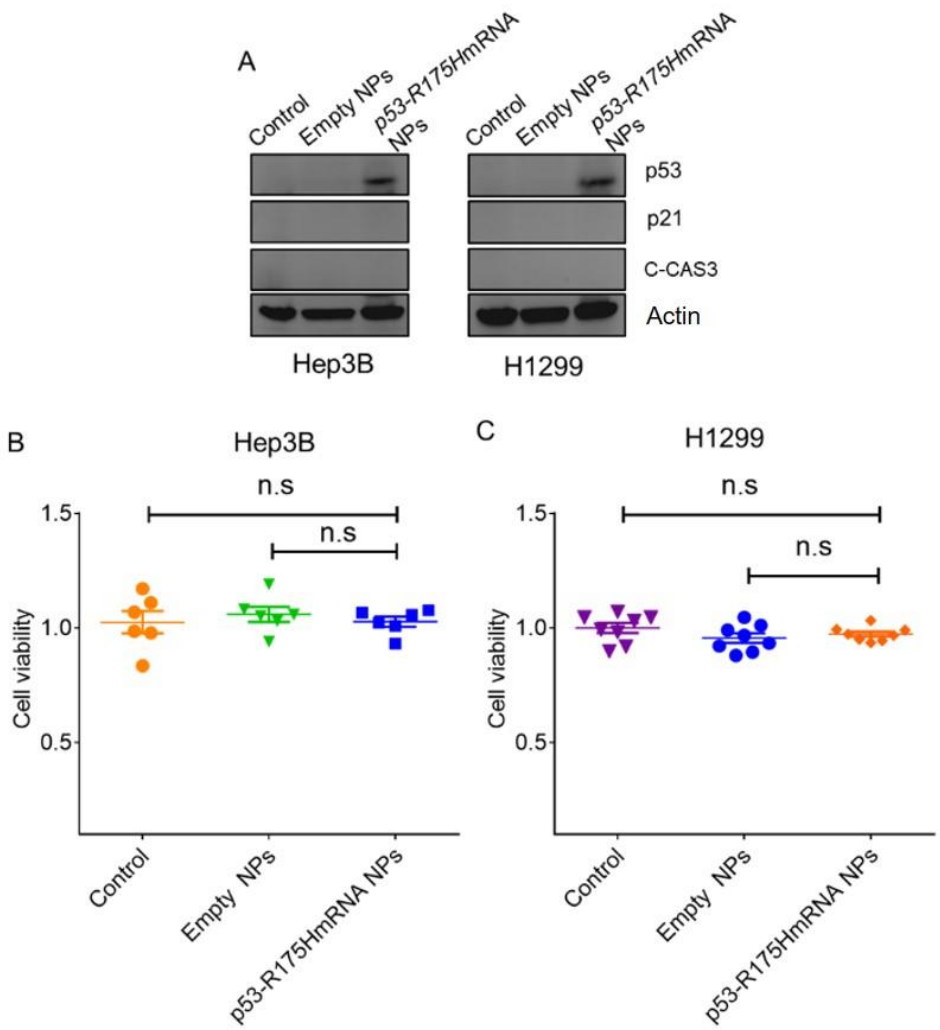

Fig. S21. In vitro toxicity of the mutant *p53-R175H*-mRNA NPs. (**A**) WB analysis of p53, p21 (cell cycle-related protein), and C-CAS3 (apoptotic marker) protein expression in both *p53*-null Hep3B cells and *p53*-null H1299 cells after treatment with *p53-R175H*-mRNA NPs. Actin was measured as the loading control. (**B**) *p53*-null Hep3B cells and (**C**) *p53*-null H1299 cells after treatment with PBS, empty NPs, or *p53-R175H*-mRNA NPs (0.830 μg/ml), as measured by AlamarBlue assay.

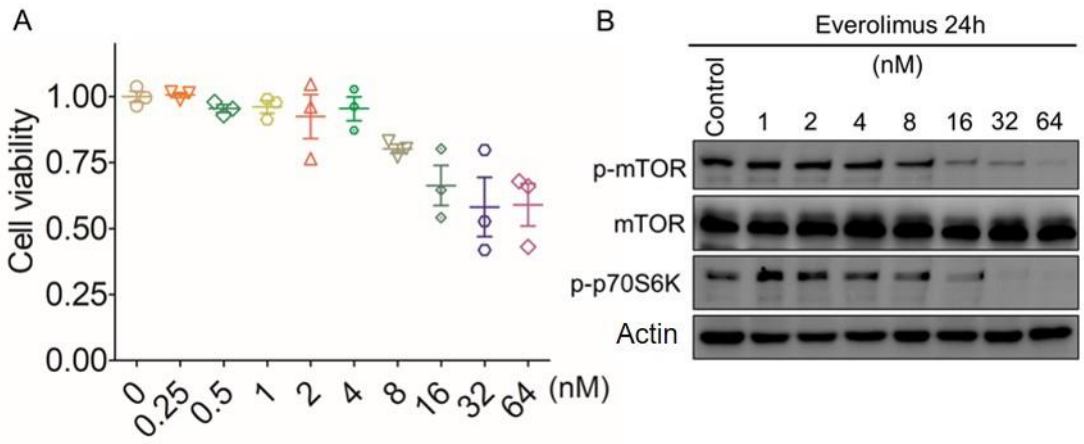

Fig. S22. Cytotoxicity of everolimus in *p53*-null H1299 cells. (**A**) Viability of H1299 cells after treatment with everolimus, as measured by AlamarBlue assay. Data shown as means ± S.E.M. (n=3). (**B**) WB analysis of total mTOR, p-mTOR, and p-p70S6K after treatment with everolimus at different concentrations. Actin was used as the loading control.

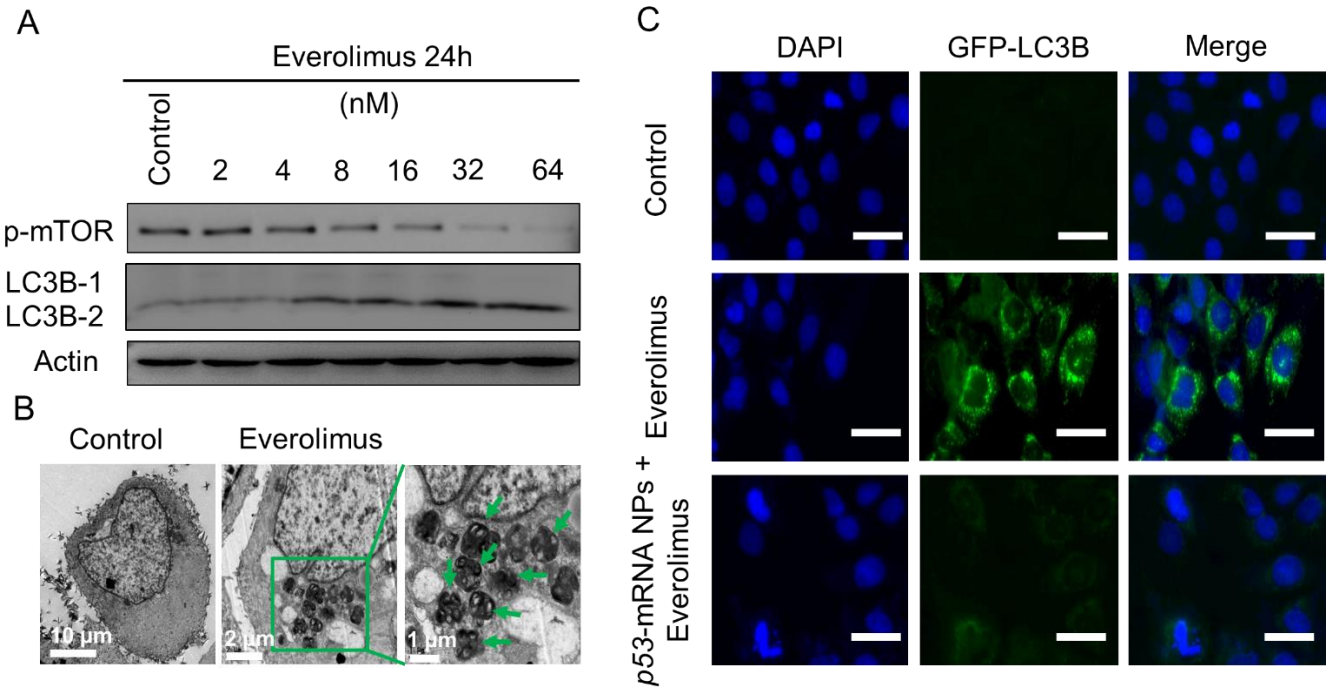

Fig. S23. Effect of everolimus on autophagy activation in *p53*-null H1299 cells. (**A**) WB analysis of p-mTOR, LC3B-1, and LC3B-2 after treatment with everolimus in H1299 cells. Actin was used as the loading control. (**B**) TEM images of H1299 cells before and after treatment with everolimus. Increased number of autophagosomes (green arrows) could be visualized after 24 h treatment of everolimus (scale bars from left to right: 10 μm, 2 μm, and 1 μm). (**C**) CLSM images of *p53*-null H1299 cells transfected with GFP-LC3B from different groups (scale bars, 50 μm). Everolimus induced autophagosomes (green), whereas co-treatment with everolimus and *p53*-mRNA NPs inhibited everolimus-induced autophagy (reduced green fluorescence).

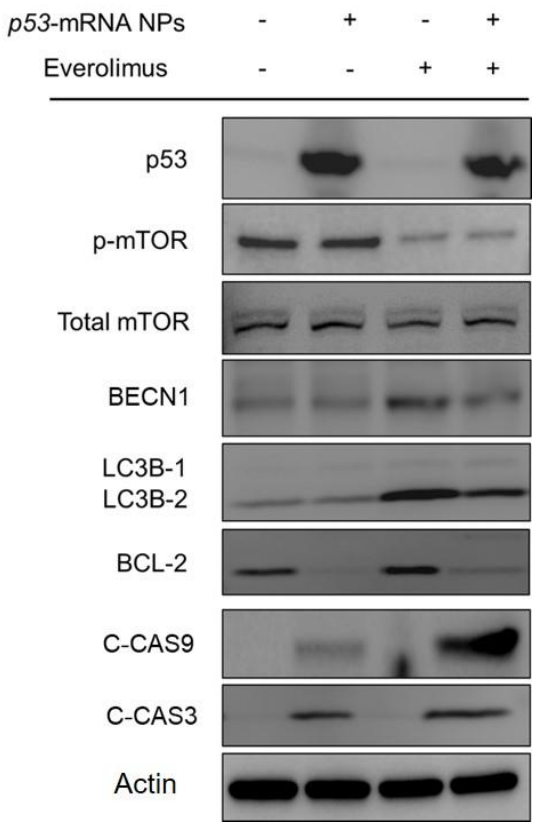

Fig. S24. WB analysis of autophagy and apoptotic signaling pathways in *p53*-null H1299 cells. p53, p-mTOR, total mTOR, BECN1, LC3B-1, LC3B-2, BCL-2, C-CAS9, and C-CAS3 in H1299 cells were assessed after different treatments. Actin was used as the loading control.

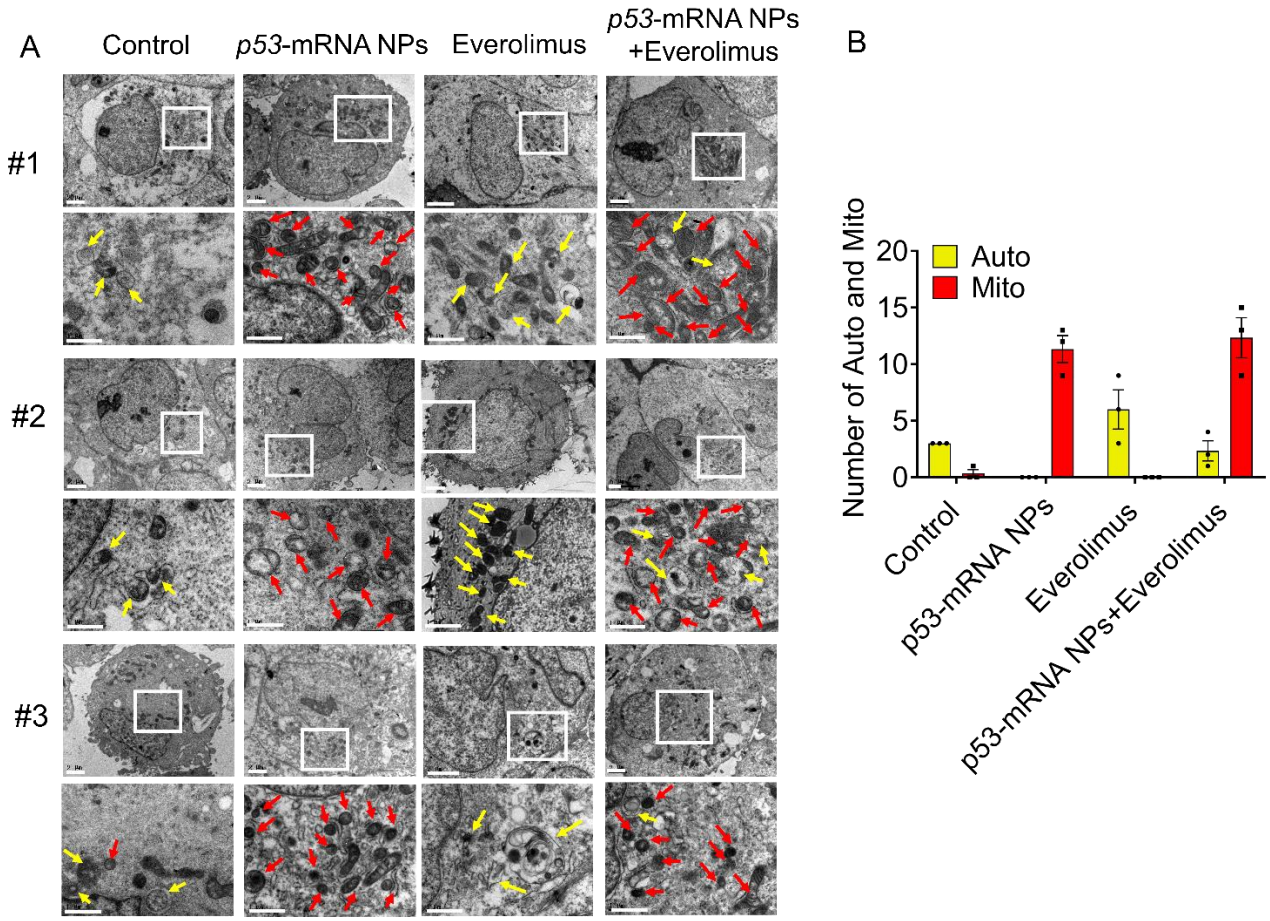

Fig. S25. Analysis of the autophagosomes and swollen mitochondria in *p53*-null H1299 cells after different treatments. (A) TEM images of the H1299 cells in control, *p53*-mRNA NPs, everolimus, and *p53*-mRNA NPs + everolimus groups (n = 3; numbers represent different batches of test). An increased number of autophagosomes (yellow arrows) could be observed after treatment with everolimus, whereas changes to mitochondria morphology (red arrows) were also seen after treatment with *p53*-mRNA NPs (scale bars, 2 μm for the raw images and 1 μm for the enlarged images). (B) Statistical analysis of the numbers of autophagosomes (yellow) and swollen mitochondria (red) after different treatments in (A).

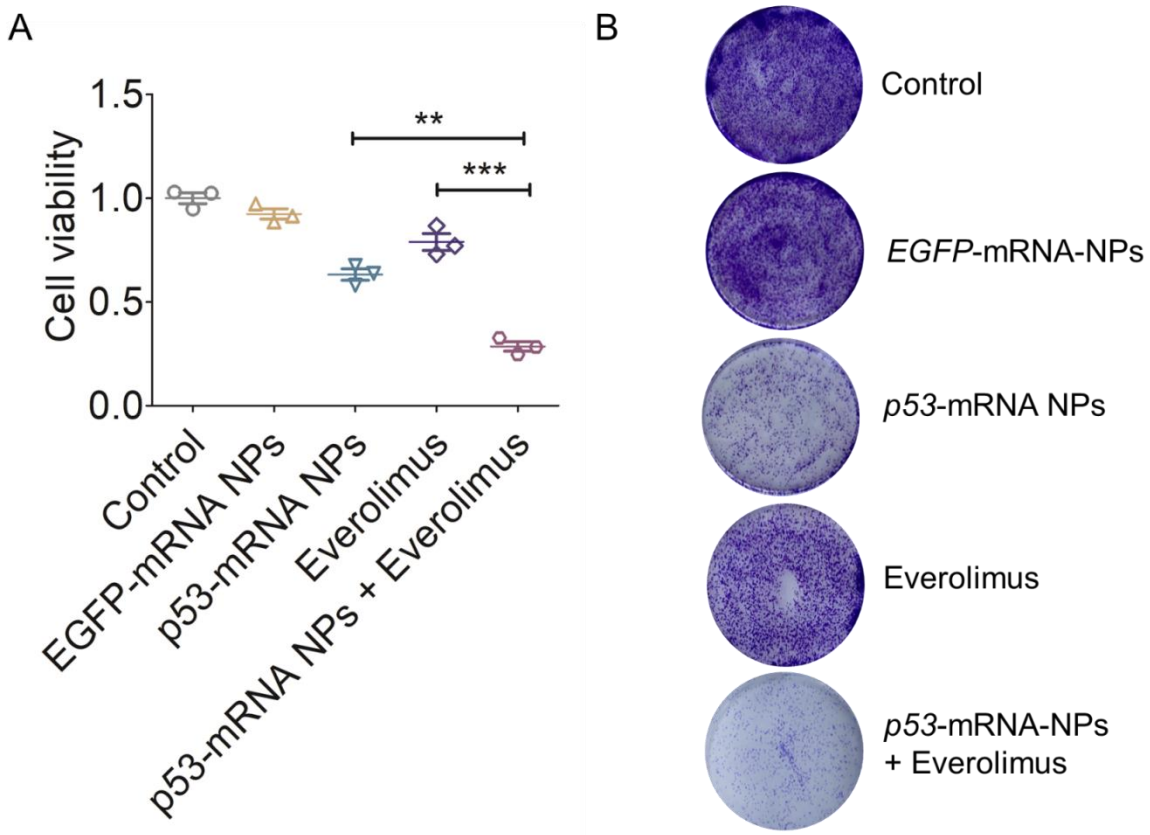

Fig. S26. In vitro therapeutic efficacy of the combination of *p53*-mRNA NPs with everolimus in *p53*-null H1299 cells. (**A**) Viability of H1299 cells in different groups (control, *EGFP*-mRNA NPs, *p53*-mRNA NPs, everolimus, or *p53*-mRNA NPs + everolimus), as measured by AlamarBlue assay. The concentration of mRNA used was 0.415 μg/ml, and the concentration of everolimus was 16 nM. Data shown as means ± S.E.M. (n=3), and statistical significance was determined using two-tailed t test (**P< 0.01, ***P< 0.001). (**B**) Colony formation of H1299 cells after different treatments in 6-well plate.

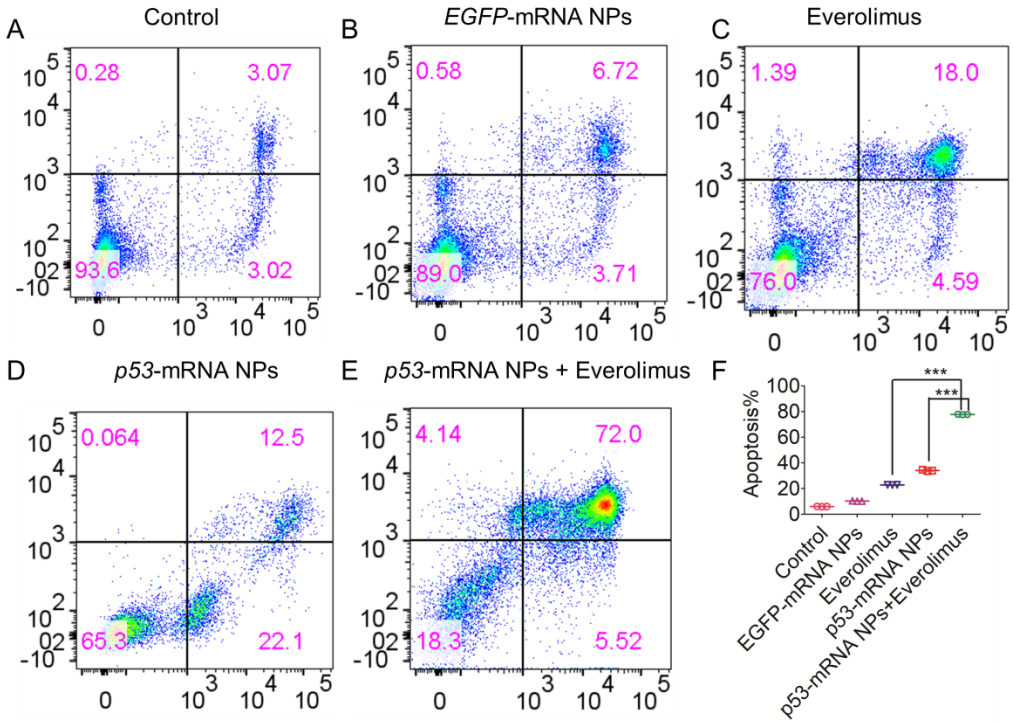

Fig. S27. In vitro apoptosis of *p53*-null H1299 cells after different treatments. Flow cytometry analysis of cell apoptosis (AnnV+PI- and AnnV+PI+) after treatment with (**A**) PBS, (**B**) *EGFP*-mRNA NPs, (**C**) *p53*-mRNA NPs, (**D**) everolimus, or (**E**) *p53*-mRNA NPs + everolimus. (**F**) Histogram of the percentage of apoptotic H1299 cells from (A-E). Data shown as means ± S.E.M. (n=3), and statistical significance was determined using two-tailed t test (***P< 0.001).

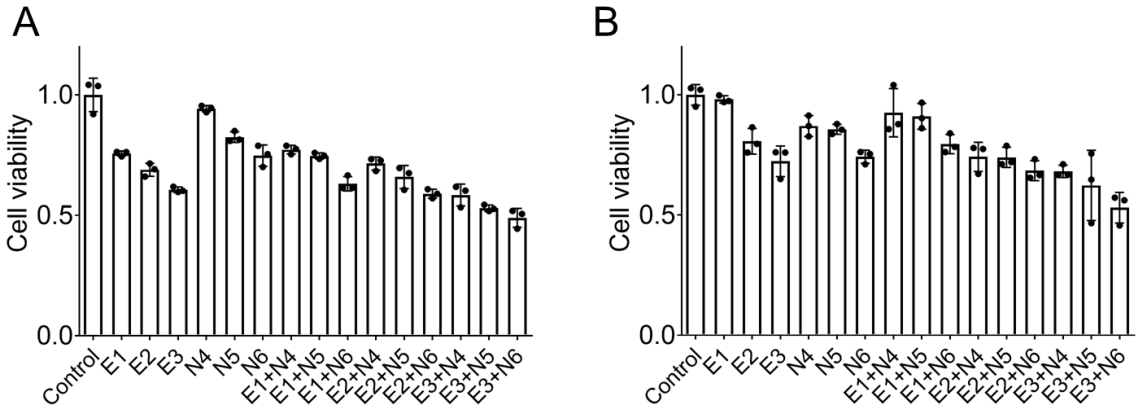

Fig. S28. In vitro toxicity of the combination of everolimus with venetoclax. Cell viability of (A) *p53*-null Hep3B cells and (B) *p53*-null H1299 cells after treatment with everolimus (Hep3B, E1: 8 nM, E2: 16 nM, and E3: 32 nM; H1299, E1: 4 nM, E2: 8 nM, and E3: 16 nM), venetoclax (N4: 40 nM, N5: 80 nM, and N6:160 nM), or the combination of both drugs, as measured by AlamarBlue assay. Data shown as means ± S.E.M. (n=3).

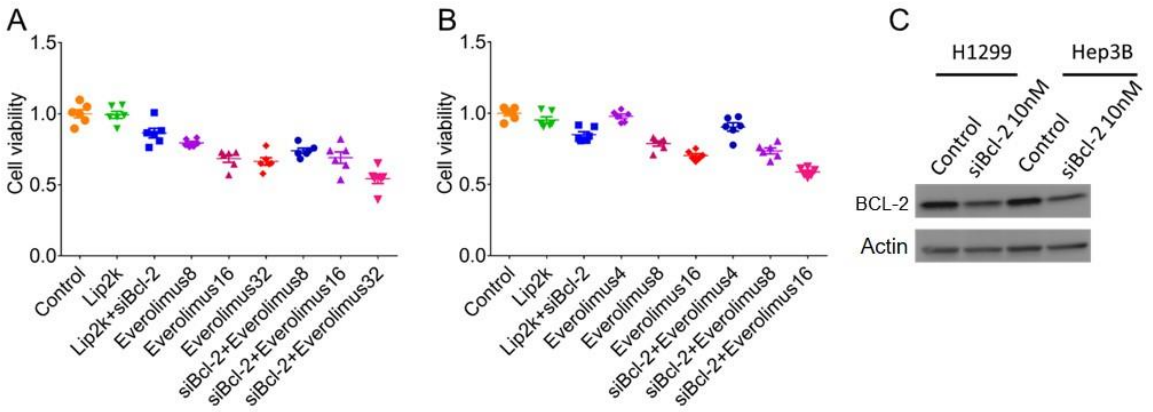

Fig. S29. In vitro toxicity of the combination of everolimus with siBcl-2. (A) Cell viability of *p53*-null Hep3B cells after treatment with PBS, lipofectamine 2000 (Lip2k), Lip2k/siBcl-2 (10 nM), everolimus (8, 16, or 32 nM), or the combination of Lip2k/siBcl-2 with everolimus, as measured by AlamarBlue assay. (B) Cell viability of *p53*-null H1299 cells after treatment with PBS, Lip2k, Lip2k/siBcl-2 (10 nM), Everolimus (4, 8, or 16 nM), or the combination of Lip2k/siBcl-2 with everolimus, as measured by AlamarBlue assay. Data shown as means ± S.E.M. (n=6). (C) WB analysis of the expression of BCL-2 in Hep3B and H1299 cells after Lip2k/siBcl-2 treatments. Actin was used as the loading control.

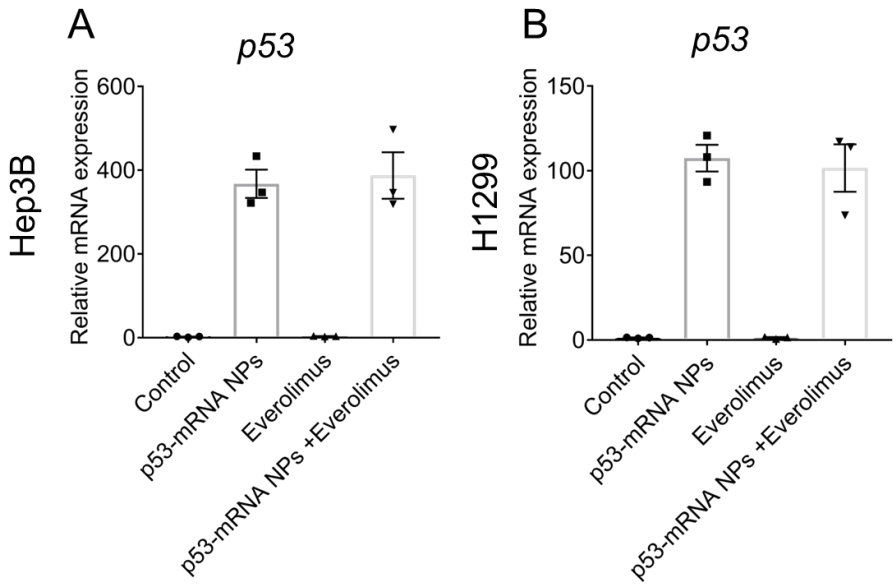

Fig. S30. The relative mRNA expression of *p53*. Cells were treated with *p53*-mRNA NPs, everolimus, or *p53*-mRNA NPs + everolimus. The relative mRNA expression of *p53* in (**A**) Hep3B and (**B**) H1299 cells was analyzed after 24 h treatment. Cells without any treatment were used as the control.

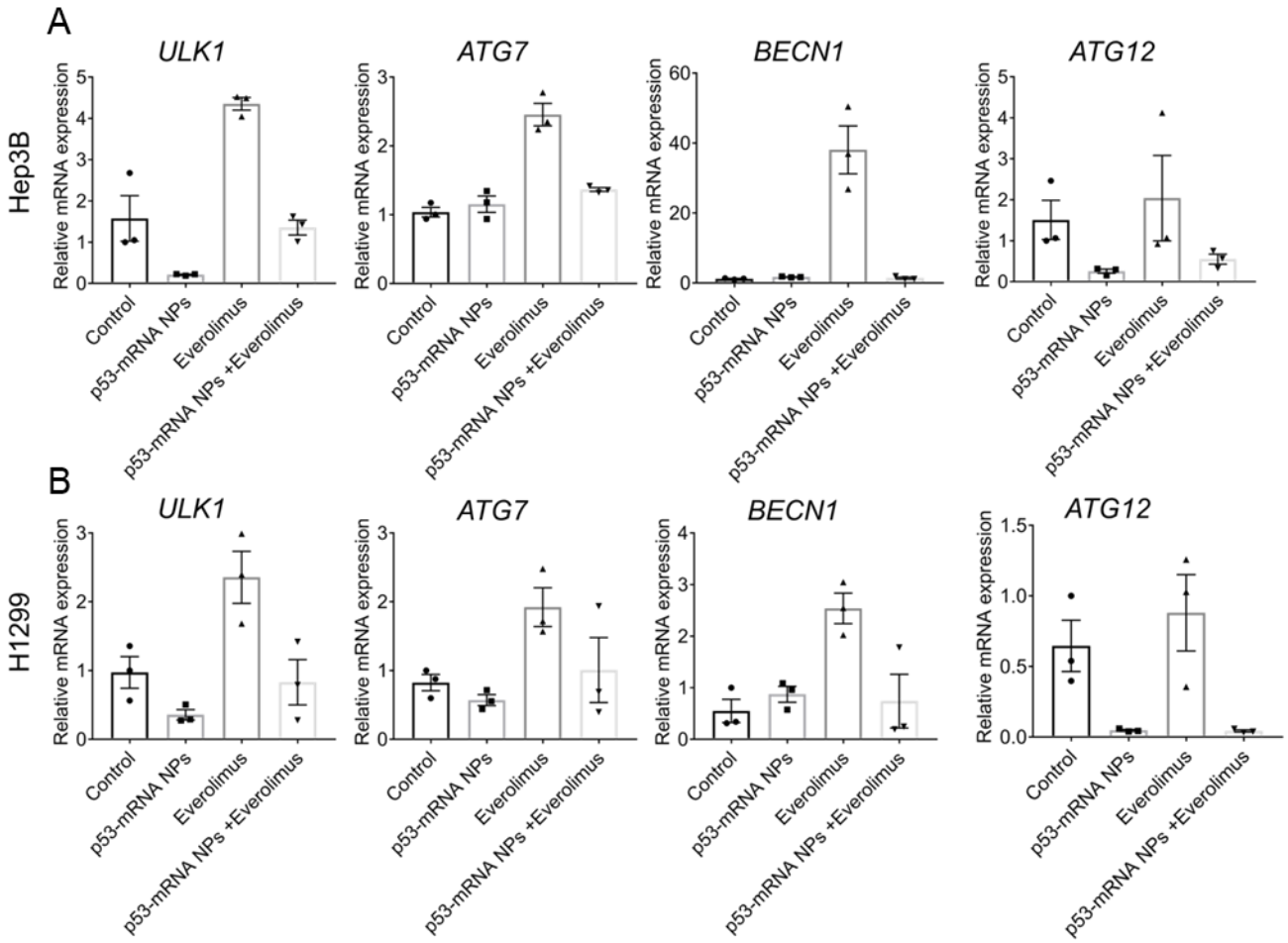

Fig. S31. The relative mRNA expression of *ULK1*, *ATG7*, *BECN1*, and *ATG12*. (**A**) Hep3B cells and (**B**) H1299 cells were analyzed after 24 h of treatment with *p53*-mRNA NPs, everolimus, or *p53*-mRNA NPs + everolimus. Cells without any treatment were used as control group.

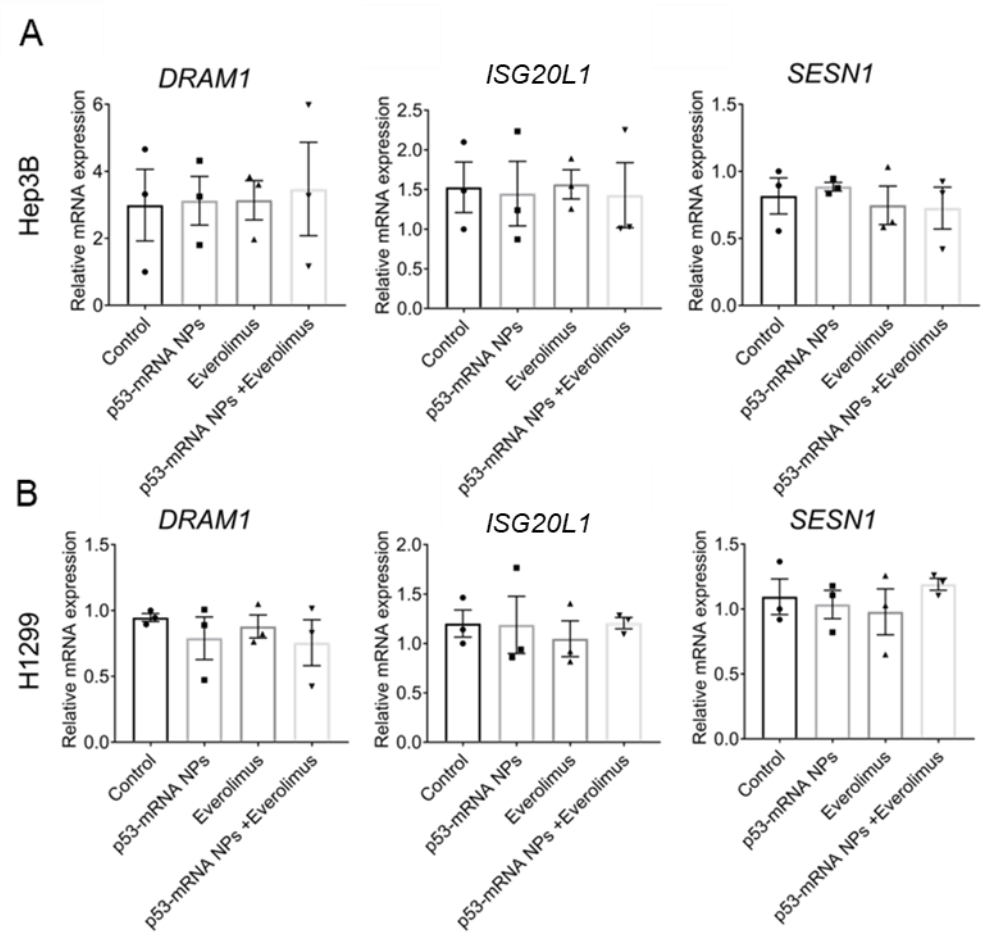

Fig. S32. The relative mRNA expression of *DRAM1, ISG20L1*, and *SESN1*. (**A**) Hep3B cells and (**B**) H1299 cells were analyzed after 24 h of treatment with *p53*-mRNA NPs, everolimus, or *p53*-mRNA NPs + everolimus. Cells without any treatment were used as control group.

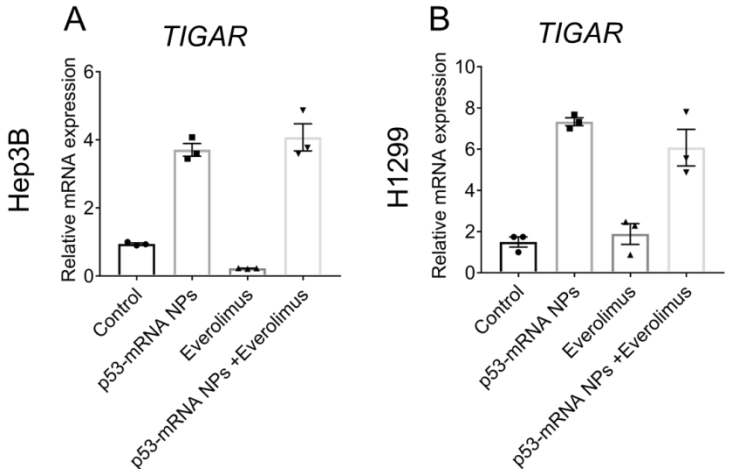

Fig. S33. The relative mRNA expression of *TIGAR*. (**A**) Hep3B and (**B**) H1299 cells were analyzed after 24 h treatment with *p53*-mRNA NPs, everolimus, or *p53*-mRNA NPs + everolimus. Cells without any treatment were used as the control.

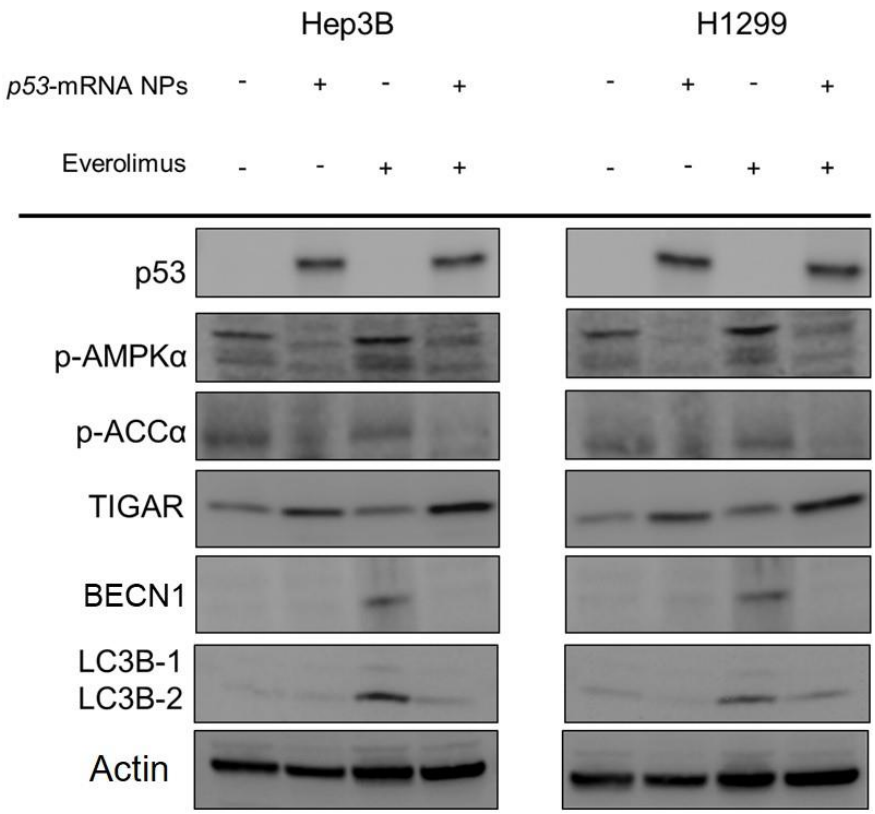

Fig. S34. WB analysis of AMPK and TIGAR pathways. p53, p-AMPKα, p-ACCα, TIGAR, BECN1, LC3B-1, and LC3B-2 in Hep3B cells (left) and H1299 cells (right) were assessed after different treatments. Actin was used as the loading control.

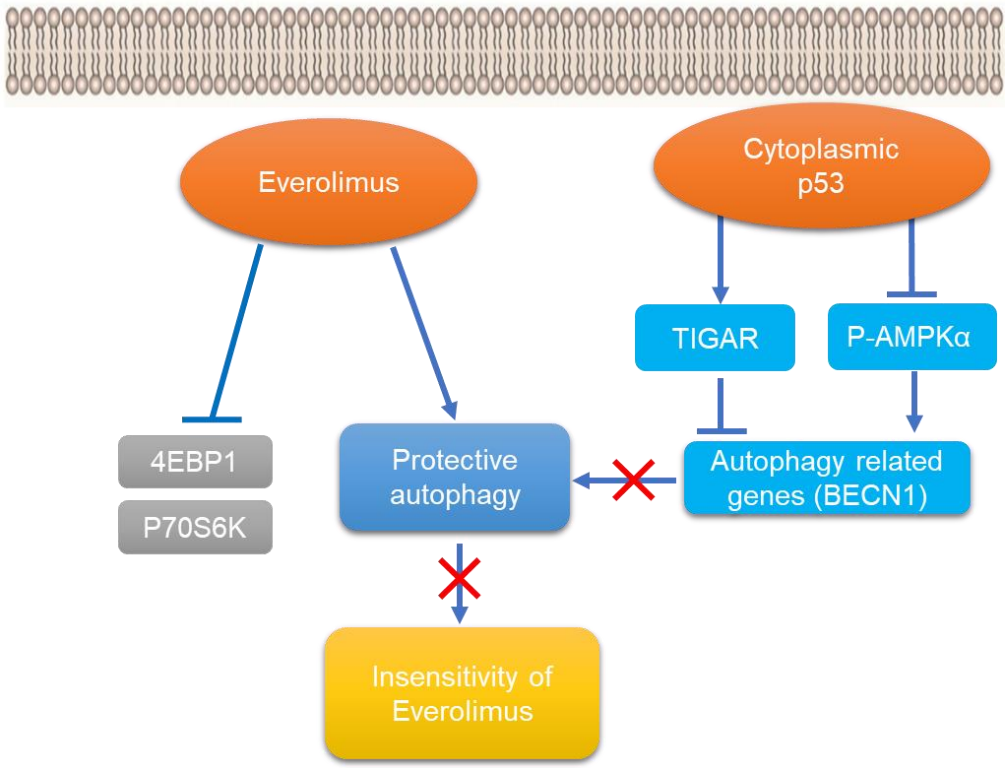

Fig. S35. Schematic representation of the possible mechanism by which p53 tumor suppressor inhibits protective autophagy and sensitizes tumor cells to everolimus.

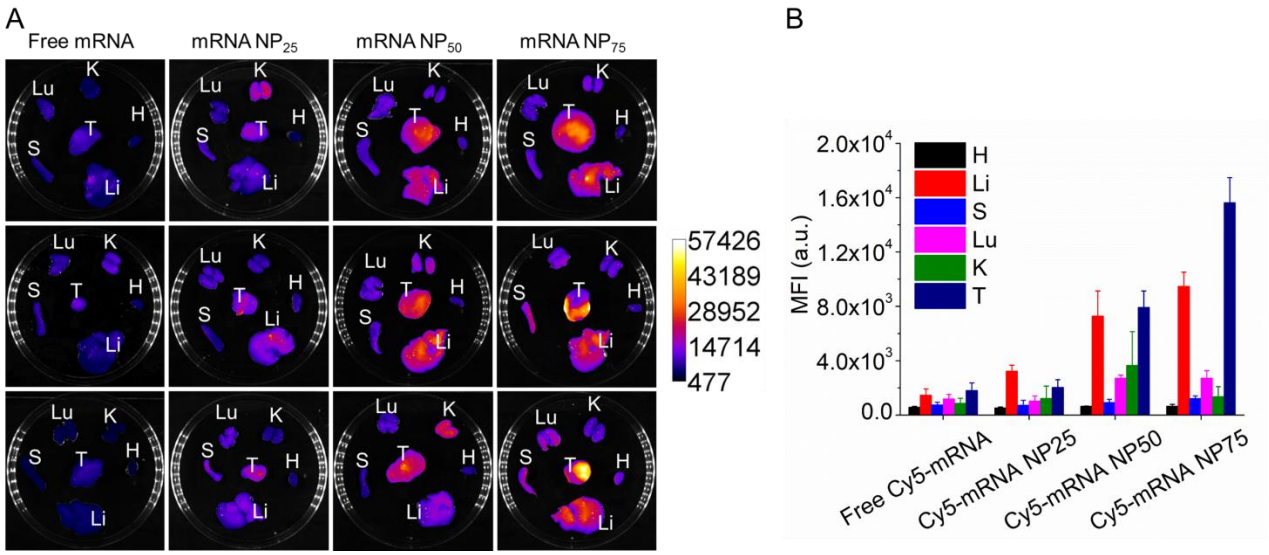

Fig. S36. BioD of different mRNA NPs in HCC xenograft tumor model. (**A**) Biodistribution of naked Cy5-labeled mRNA and Cy5-labeled mRNA NPs in different organs (H: heart Li: liver, S: spleen, Lu: lungs, and K: kidneys) and Hep3B tumors. NP_{25}, NP_{50}, and NP_{75} represent three different ratios of DSPE-PEG/DMPE-PEG in the lipid-PEG layer of hybrid mRNA NPs. (**B**) Quantification of biodistribution of naked Cy5-labeled mRNA and Cy5-labeled mRNA NPs from (A). Data shown as means ± S.E.M. (n=3).

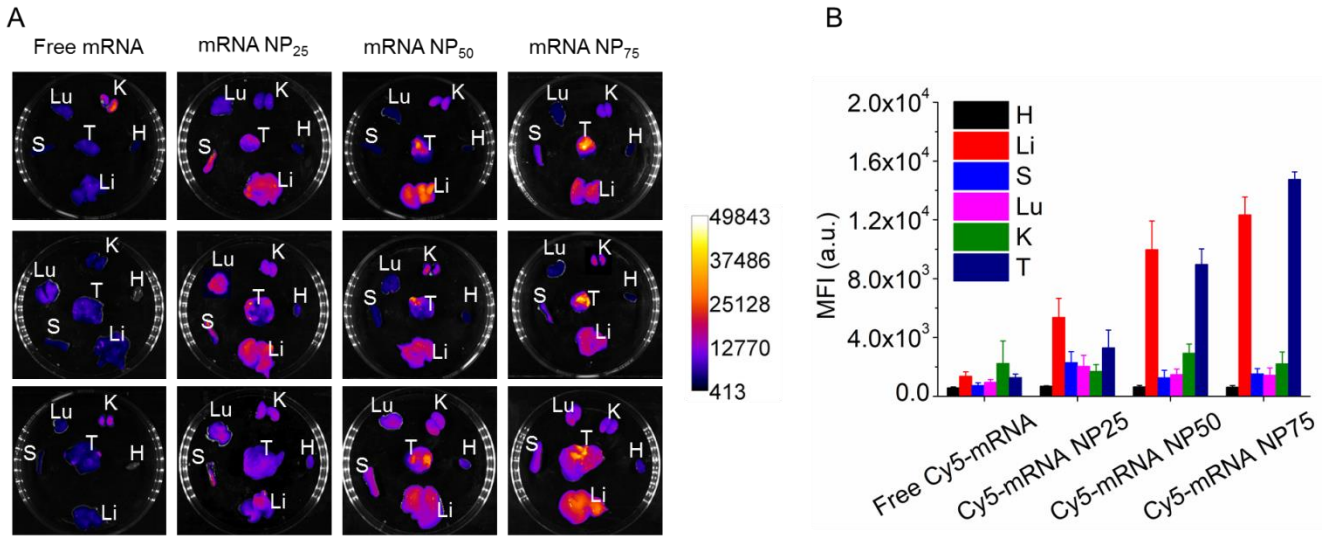

Fig. S37. BioD of different mRNA NPs in NSCLC xenograft tumor model. (**A**) Biodistribution of naked Cy5-labeled mRNA and Cy5-labeled mRNA NPs in different organs (H: heart, Li: liver, S: spleen, Lu: lungs, and K: kidneys) and H1299 tumors. NP_{25}, NP_{50}, and NP_{75} represent three different ratios of DSPE-PEG/DMPE-PEG in the lipid-PEG layer of hybrid mRNA NPs. (**B**) Quantification of biodistribution of naked Cy5-labeled mRNA and Cy5-labeled mRNA NPs from (A). Data shown as means ± S.E.M. (n=3).

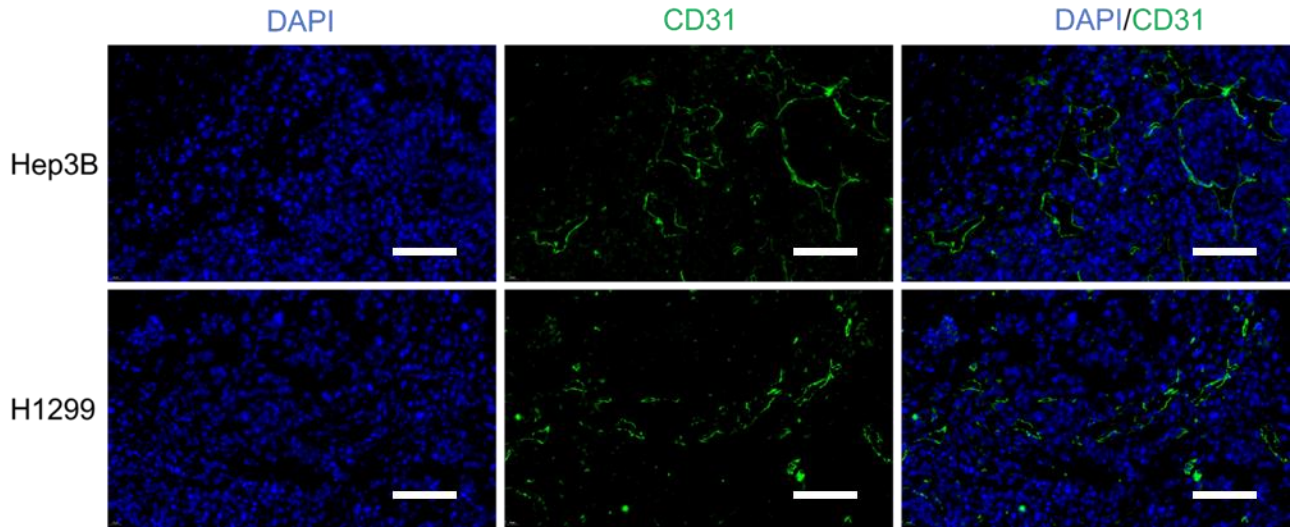

Fig. S38. Blood vessel staining in tumor sections. CLSM images of the tumor sections from the *p53*-null HCC xenograft model and *p53*-null NSCLC xenograft model (scale bar, 400 μm). The nuclei of tumor cells were stained by DAPI (blue), and the blood vessels were stained by anti-CD31 (green).

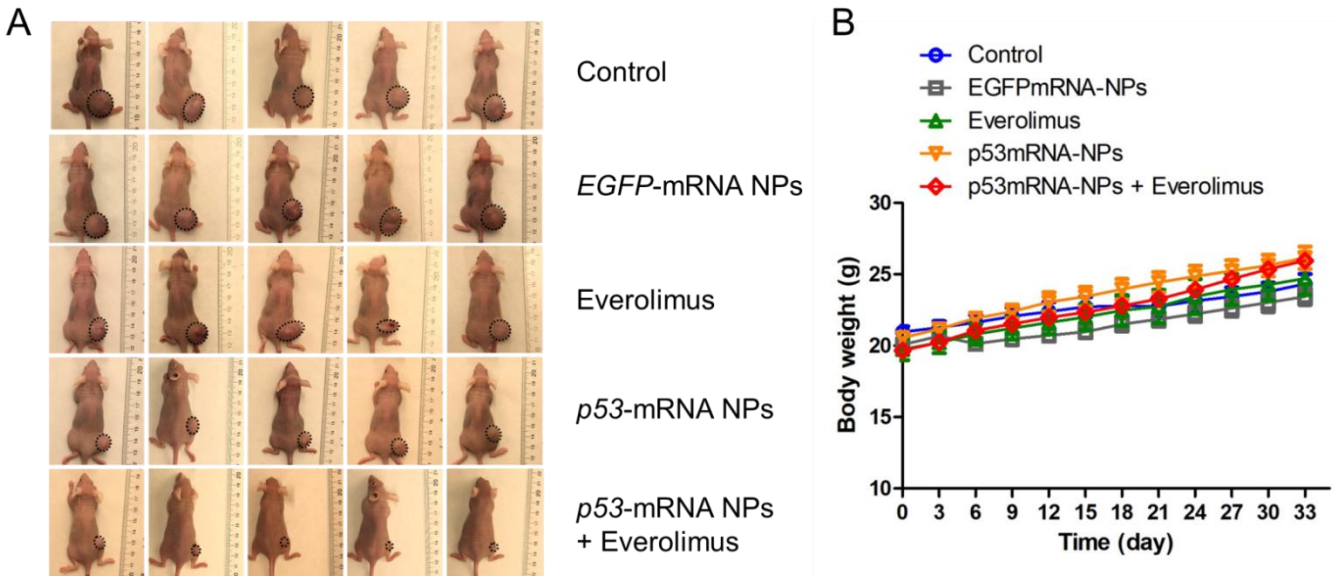

Fig. S39. Efficacy and safety of different treatments in HCC xenograft model. (**A**) Whole-body images of mice bearing *p53*-null Hep3B xenograft tumors treated with PBS, *EGFP*-mRNA NPs, everolimus, *p53*-mRNA NPs, or *p53*-mRNA NPs + everolimus (Day 35). (**B**) Average body weight of Hep3B tumor-bearing mice over the course of therapy. Data shown as means ± S.E.M. (n=5).

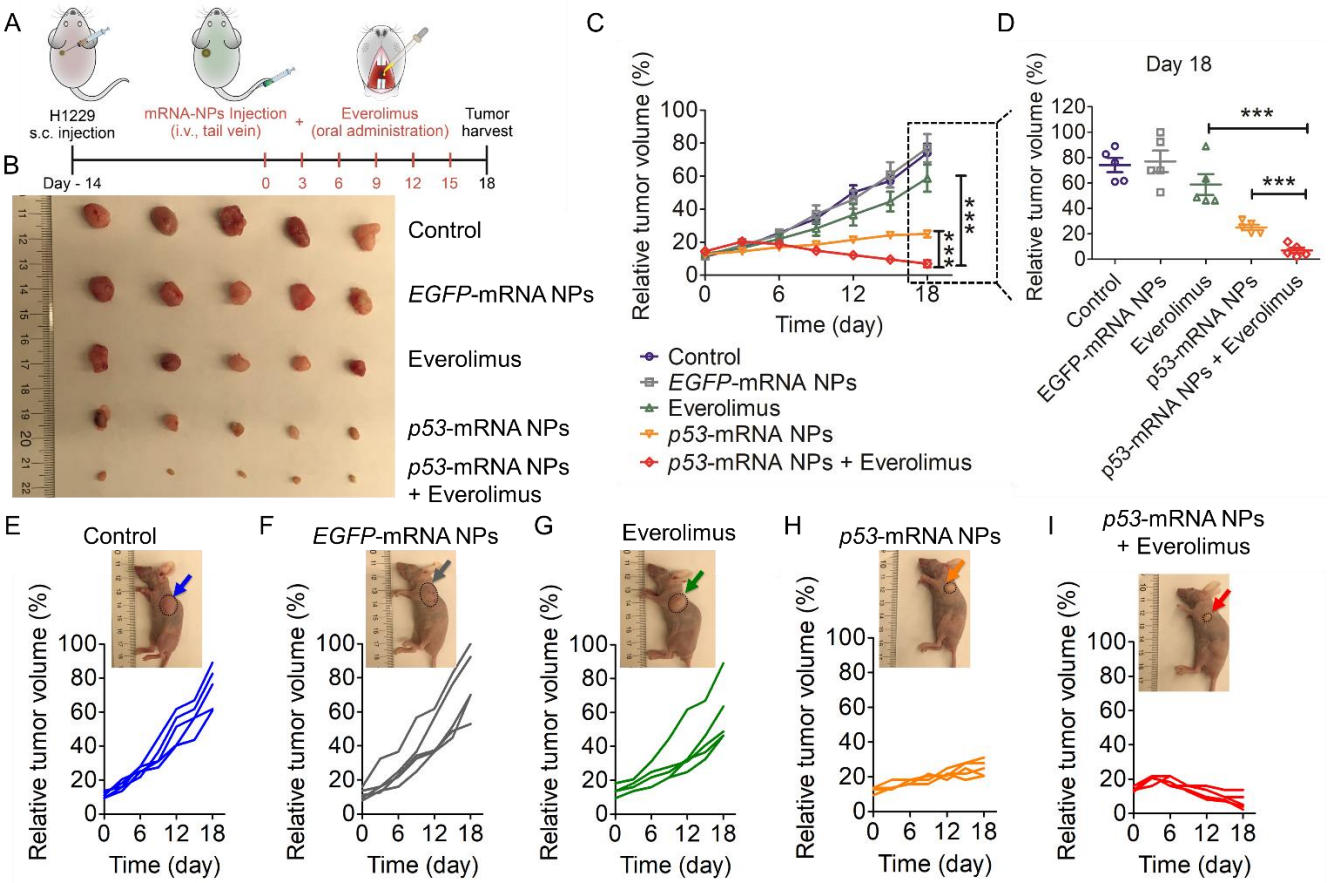

Fig. S40. Antitumor effects of *p53*-mRNA NPs are synergistic with everolimus in NSCLC xenograft model. (**A**) Scheme of tumor inoculation (s.c.) and treatment schedule in H1299 tumor-bearing athymic nude mice. Fourteen days after tumor inoculation, mice were treated with PBS (IV), *EGFP*-mRNA NPs (IV), *p53*-mRNA NPs (IV), everolimus (oral), or *p53*-mRNA NPs (IV) + everolimus (oral) every three days for 6 rounds (mRNA dose: 750 μg/kg; everolimus dose: 5 mg/kg). Tumors from different groups were harvested three days after the final treatment. (**B**) Photos of excised tumors from mice bearing H1299 xenografts in different treatment groups on Day 18 (n=5). (**C**) Average tumor growth kinetics for all treatment groups. Data shown as means ± S.E.M. (n=5), and significance was determined using two-tailed t test (***P< 0.001). (**D**) Average tumor volumes at the experimental endpoint (Day 18) in all groups. Data shown as means ± S.E.M. (n=5), and statistical significance was determined using two-tailed t test (***P< 0.001). (**E-I**) Individual tumor growth kinetics in the (**E**) control, (**F**) *EGFP*-mRNA NPs, (**G**) everolimus, (**H**) *p53*-mRNA NPs, and (**I**) *p53*-mRNA NPs + everolimus groups (n=5). Insets: Representative mouse photographs at the experimental endpoint (Day 18). The arrows indicate the tumors on mice.

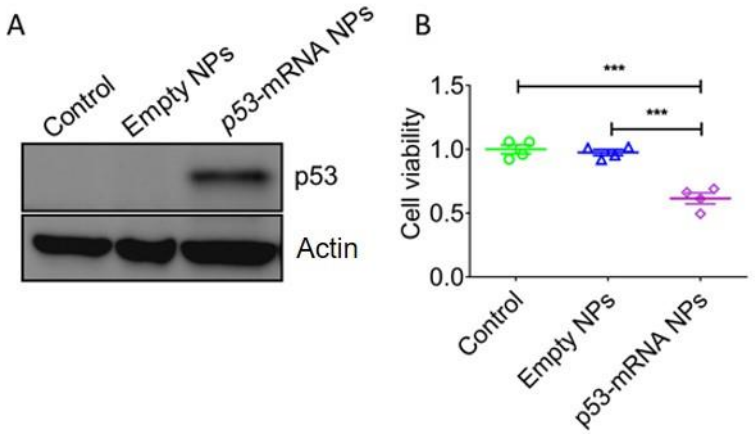

Fig. S41. Murine p53 restoration in *p53*-null murine liver cancer RIL-175 cells. (A) WB analysis of the expression of mouse p53 protein after treatment with murine *p53*-mRNA NPs. Actin was used as the loading control. (B) Viability of *p53*-null murine liver cancer cell RIL-175 after treatment with empty NPs or murine *p53*-mRNA NPs (0.830 μg/ml), as measured by AlamarBlue assay. Data shown as means ± S.E.M. (n=4), and statistical significance was determined using two-tailed t test (***P< 0.001).

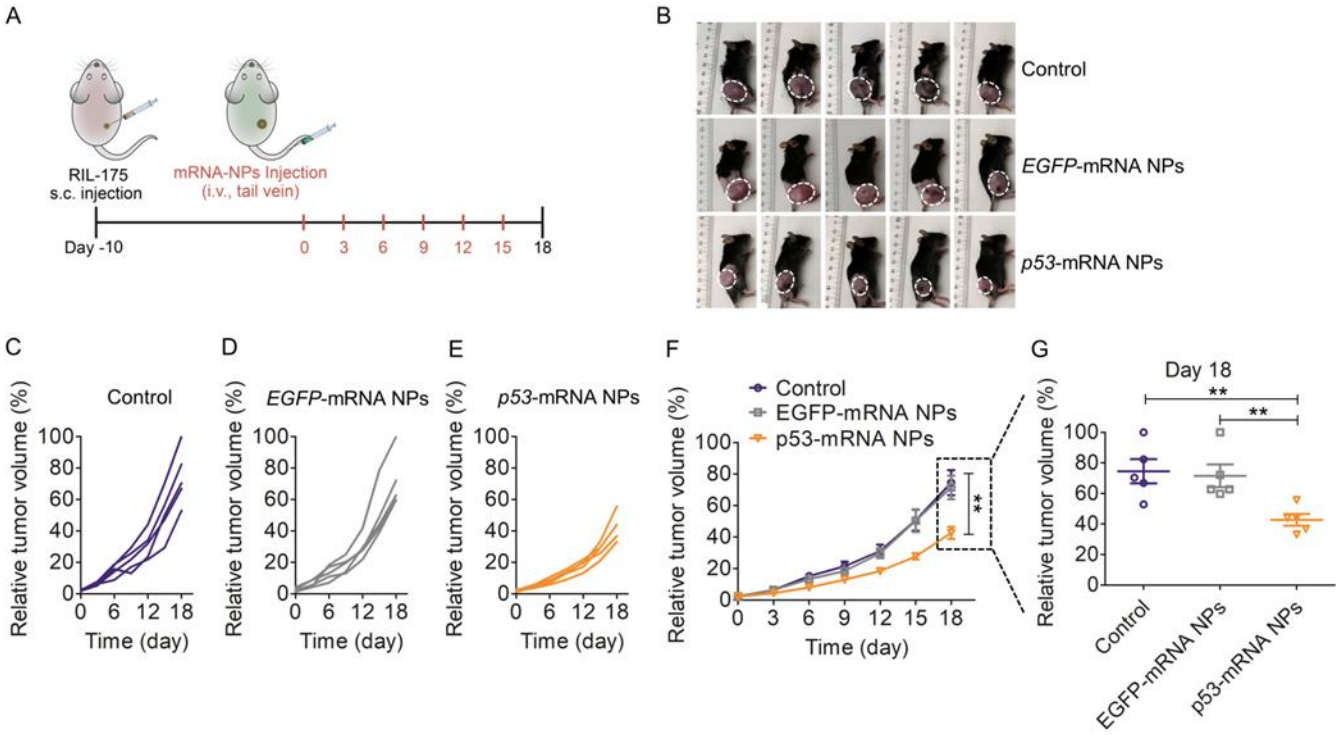

Fig. S42. Therapeutic efficacy of murine *p53*-mRNA NPs in immunocompetent mice bearing *p53*-null RIL-175 tumors. (A) Scheme of tumor inoculation (s.c.) and treatment schedule in RIL-175 tumor-bearing C57BL/6 mice. Ten days after tumor inoculation, mice were treated with PBS (IV), *EGFP*-mRNA NPs (IV), or murine *p53*-mRNA NPs (IV) every three days for 6 rounds (at an mRNA dose of 750 μg per kg of animal weight). (B) Whole-body images of immunocompetent mice bearing *p53*-null RIL-175 liver tumors treated with PBS, *EGFP*-mRNA NPs, or murine *p53*-mRNA NPs (Day

18). (C-E) Individual tumor growth kinetics in the (C) control, (D) EGFP-mRNA NPs, and (E) murine *p53*-mRNA NPs groups (n=5). (F) Average tumor growth kinetics for all treatment groups. Data shown as means ± S.E.M. (n=5), and significance was determined using two-tailed t test (**P< 0.01). (G) Average tumor volumes at the experimental endpoint (Day 18) in all groups. Data shown as means ± S.E.M. (n=3), and statistical significance was determined using two-tailed t test (**P< 0.01).

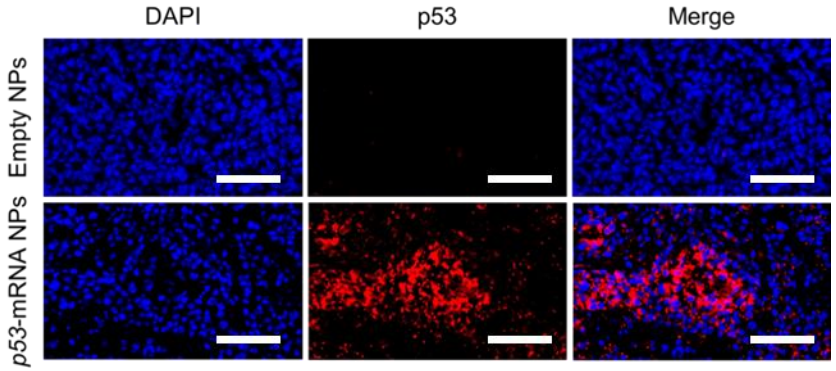

Fig. S43. Expression of p53 protein in HCC xenograft model after treatment with *p53*-mRNA NPs. IF images of p53 (red) and nucleus (blue) co-stained in Hep3B tumor sections at 12 h after IV injection of *p53*-mRNA NPs. Empty NPs were used as control group (scale bars, 300 μm).

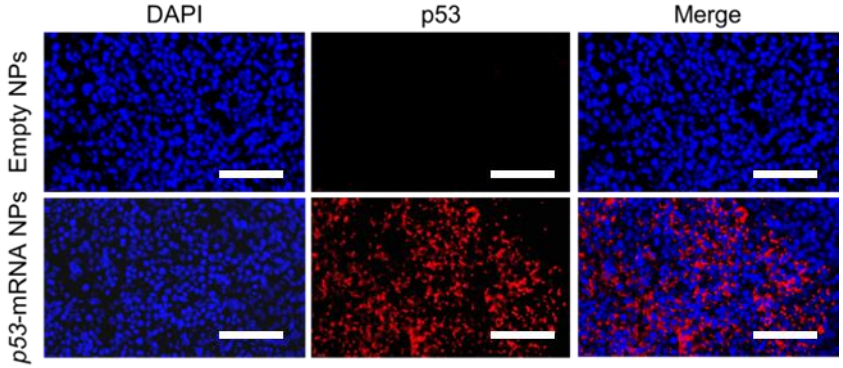

Fig. S44. Expression of p53 protein in NSCLC xenograft model after treatment with *p53*-mRNA NPs. IF images of p53 (red) and nucleus (blue) co-stained in H1299 tumor sections at 12 h post IV injection of *p53*-mRNA NPs. Empty NPs was used as control group (scale bars, 300 μm).

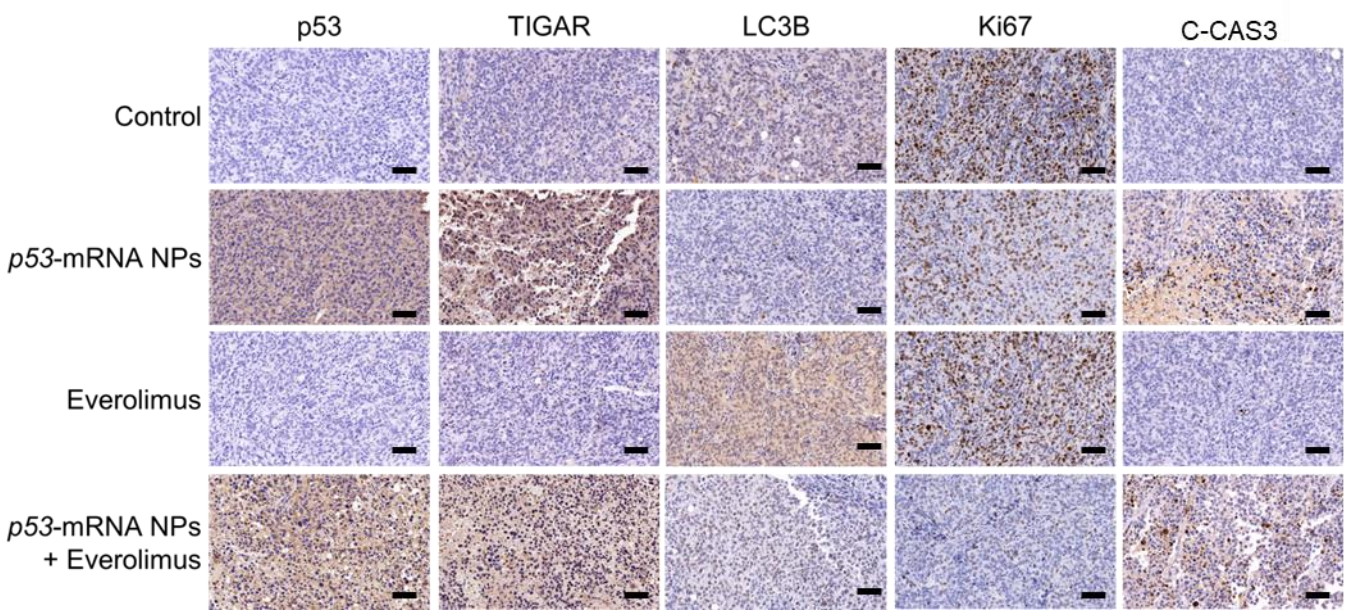

Fig. S45. IHC images from tumor sections of H1299 tumor–bearing mice before and after treatment with *p53*-mRNA NPs. The protein expressions of p53, TIGAR, LC3B, Ki67, and C-CAS3 were evaluated by IHC staining (blue: nucleus; brown: p53, TIGAR, LC3B, Ki67, or C-CAS3; scale bars, 100 μm).

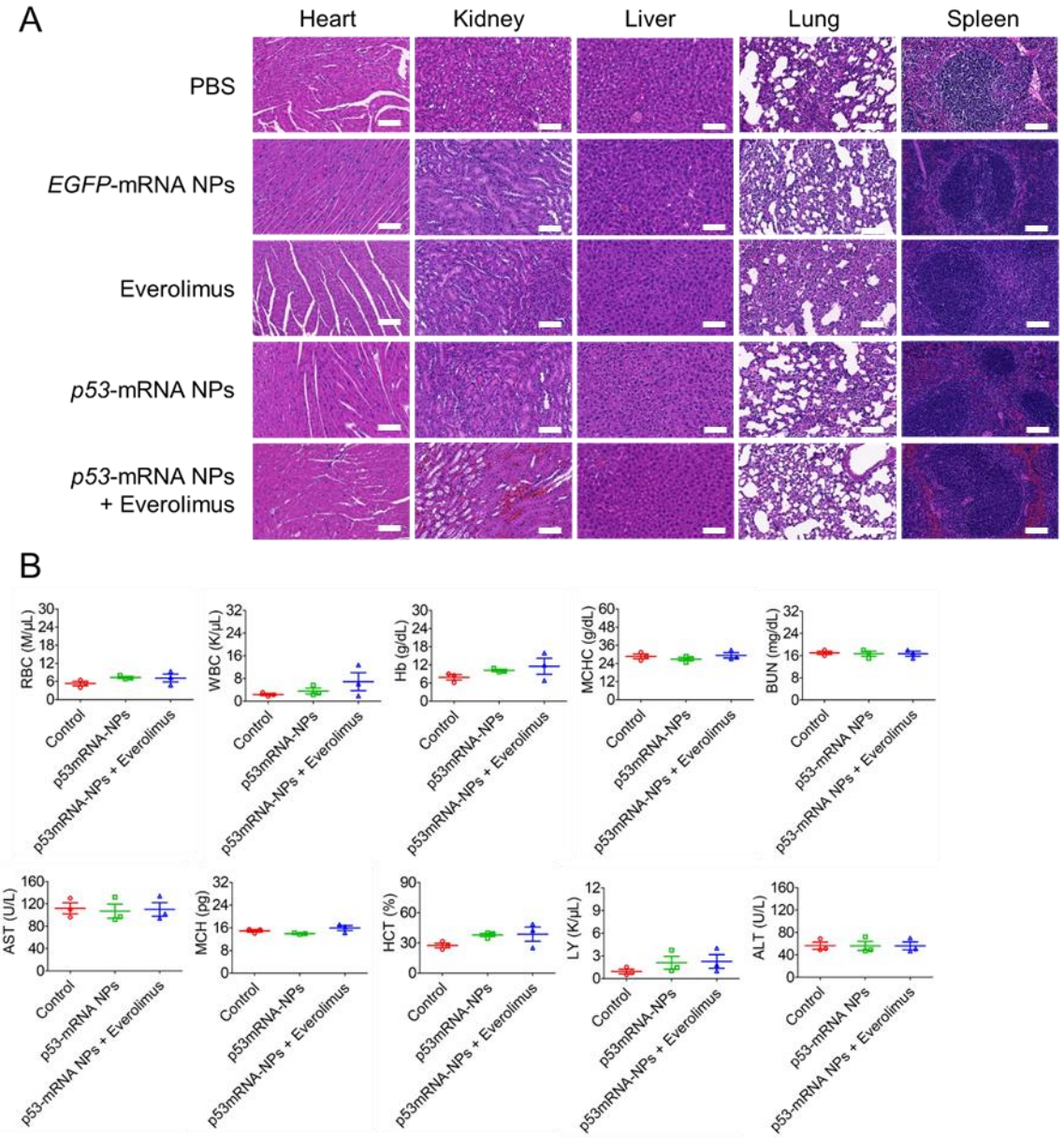

Fig. S46. In vivo toxicity of the *p53*-mRNA NP–mediated strategy for everolimus rescue assessed by histopathological and hematological analysis. (**A**) H&E staining of sections of the major organs (heart, liver, spleen, lung, and kidney) was performed three days after the last administration of PBS, *EGFP*-mRNA NPs, everolimus, *p53*-mRNA NPs, or *p53*-mRNA NPs + everolimus (scale bars, 100 μm). (**B**) Analysis of serum biochemistry and whole blood parameters: alanine aminotransferase (ALT), aspartate aminotransferase (AST), urea nitrogen (BUN), red blood cells (RBC), white blood cells (WBC), hemoglobin (Hb), mean corpuscular hemoglobin concentration (MCHC), mean corpuscular hemoglobin (MCH), hematocrit (HCT), and lymphocyte count (LY).

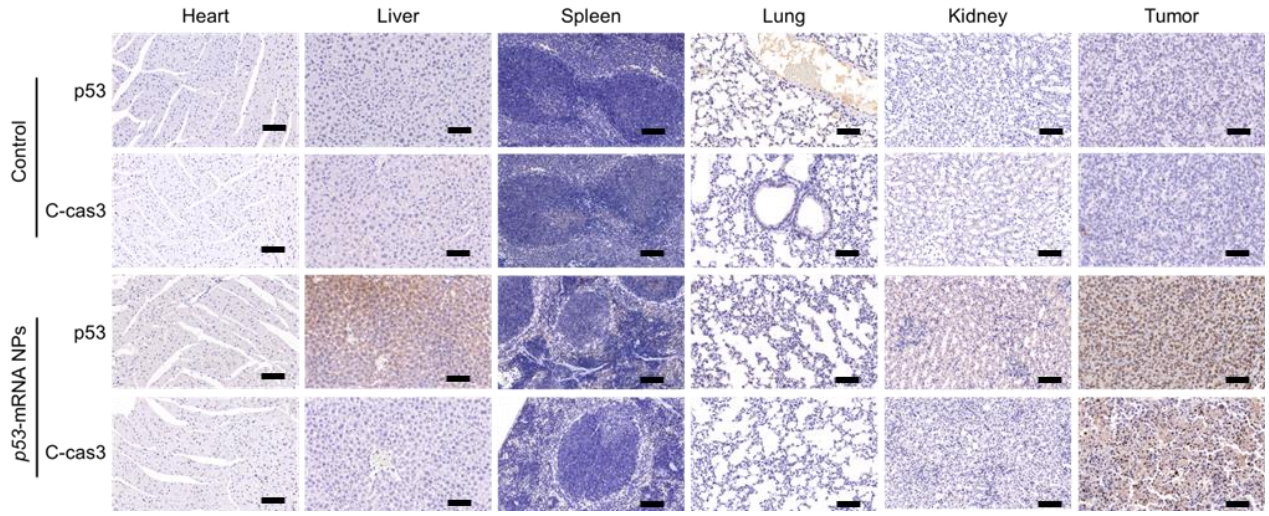

Fig. S47. IHC images from major organs and tumor sections of the HCC xenograft model. The protein expressions of p53 and apoptotic marker (C-cas3) were evaluated by IHC staining (blue: nucleus; brown: p53 or C-cas3) with or without the treatment of *p53*-mRNA NPs (scale bars, 100 μm).

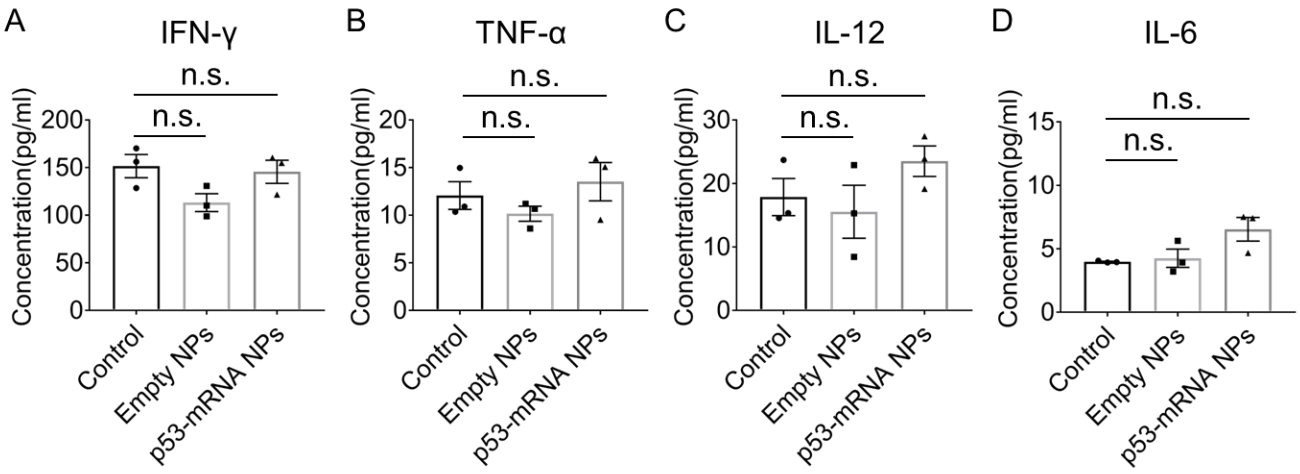

Fig. S48. Evaluation of immune responses after the treatment with mRNA NPs. Serum concentrations of (**A**) IFN-γ, (**B**) TNF-α, (**C**) IL-12, and (**D**) IL-6 at 24 h after injection of PBS, empty NPs, or *p53*-mRNA NPs in immunocompetent BALB/c mice.

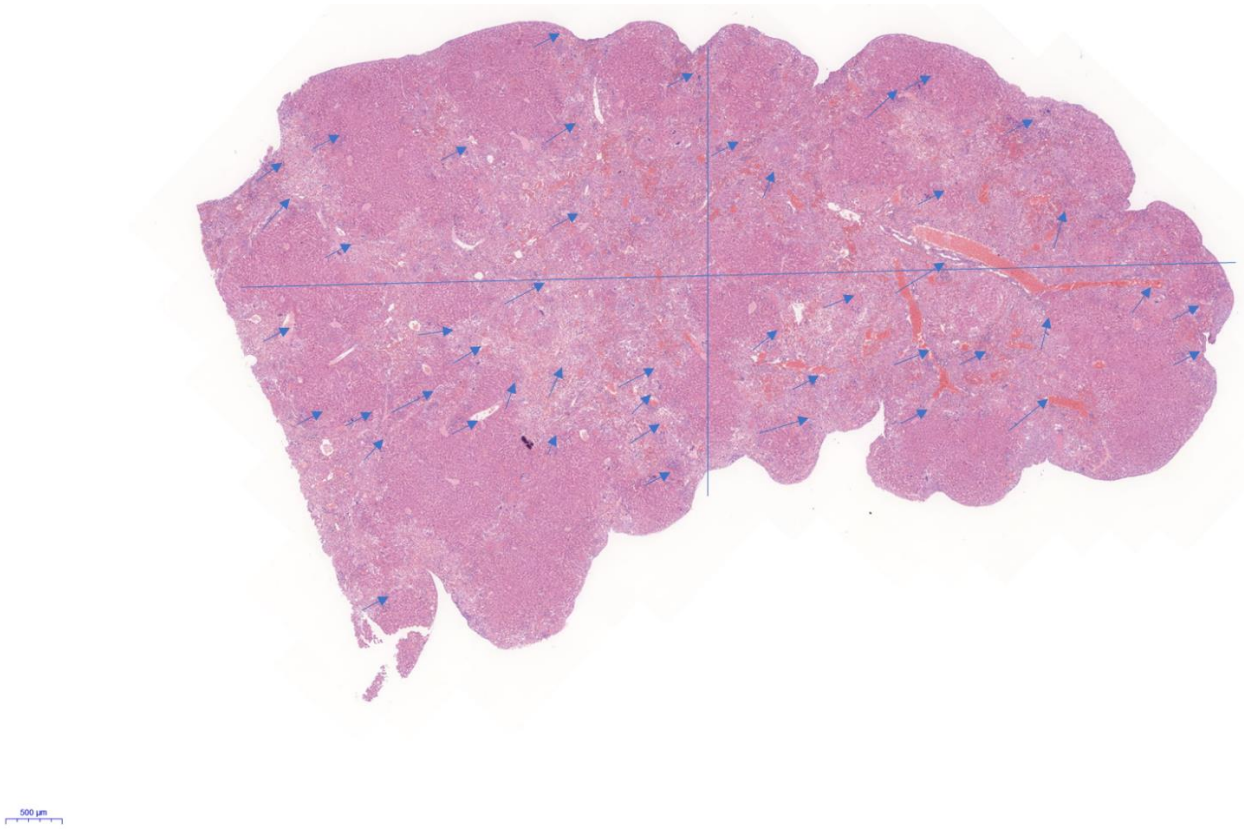

(A) PBS Group

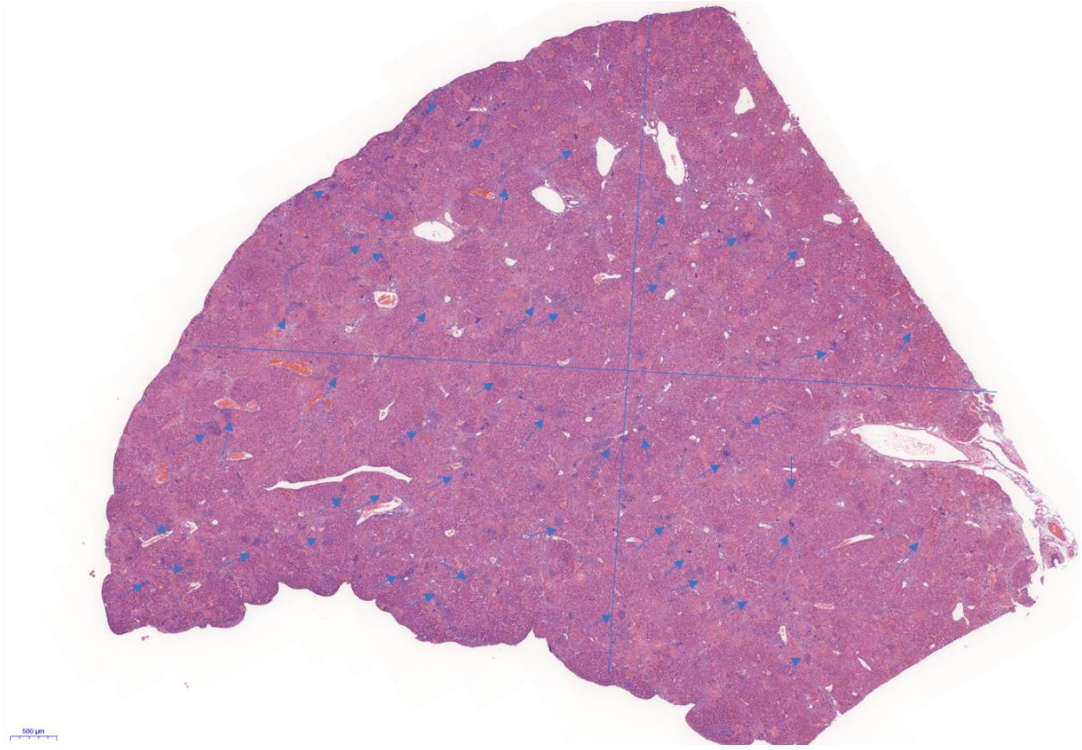

(B) *EGFP*-mRNA NPs Group

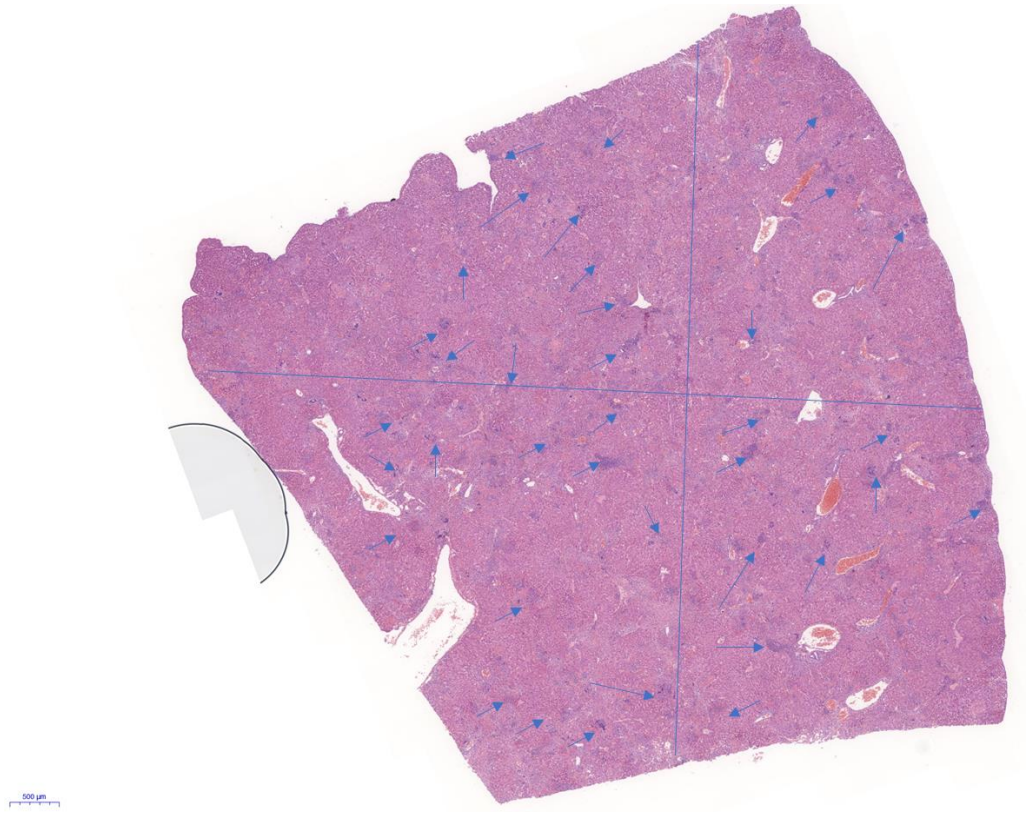

(C) Everolimus Group

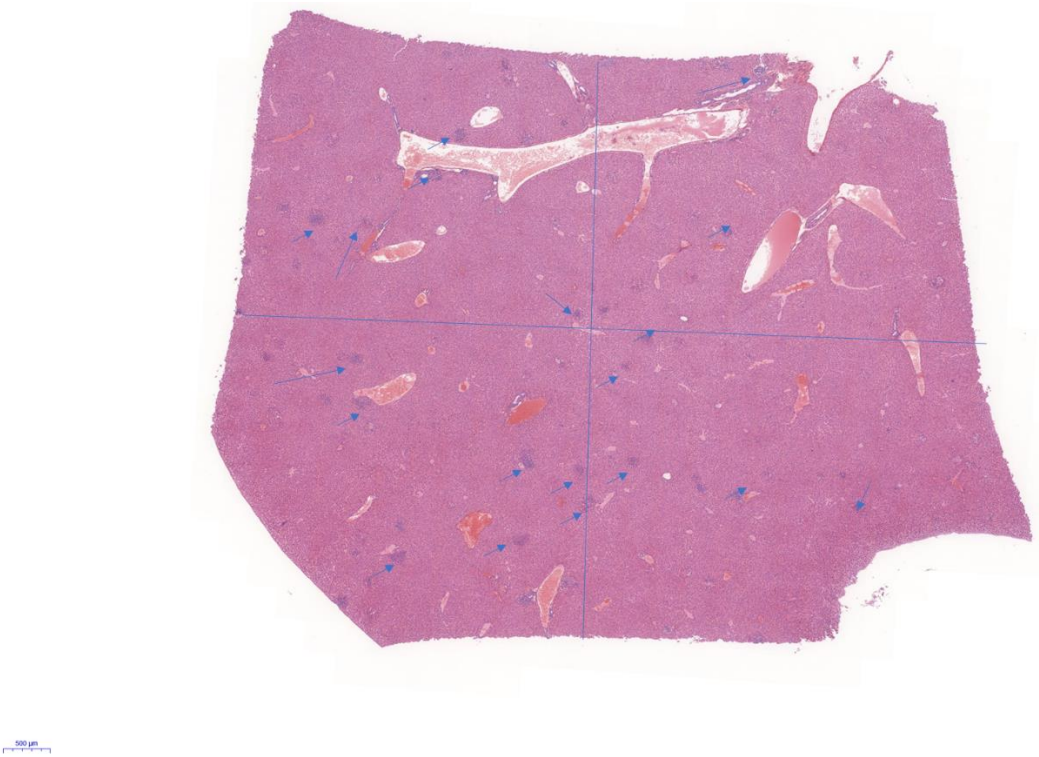

(D) *p53*-mRNA NPs Group

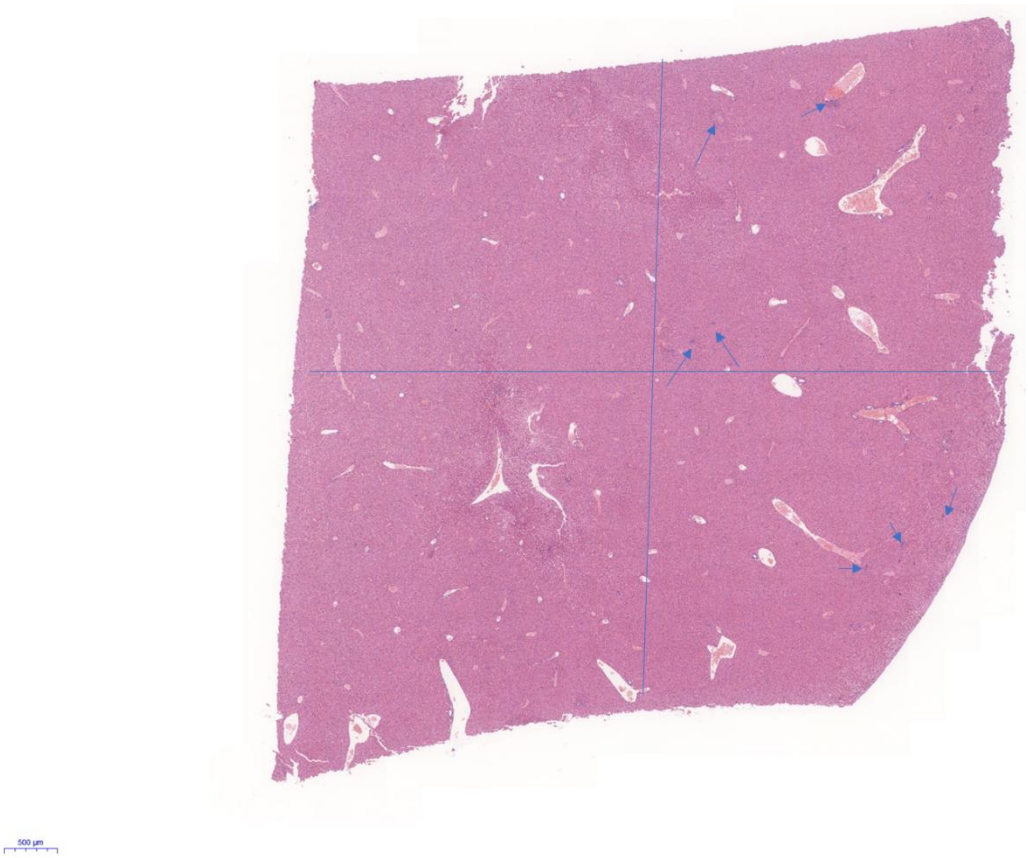

(E) *p53*-mRNA NPs + Everolimus Group

Fig. S49. Scans of the liver metastases from different treatment groups in Fig. 6. The five groups include (A) PBS control, (B) *EGFP*-mRNA NPs, (C) Everolimus, (D) *p53*-mRNA NPs, and (E) *p53*-mRNA NPs + Everolimus.

SUPPLEMENTARY TABLES

Table S1. Compositions of different NP formulations.

NP formulations	Weight (μg)				Classification
	mRNA/G0-C14 (ratio)	PDSA	DSPE-PEG	DMPE-PEG	
NP1	24/240 (1:10)	4000	700	2100	NP_{25a}
NP2*	24/360 (1:15)	4000	700	2100	NP_{25}
NP3	24/480 (1:20)	4000	700	2100	NP_{25b}
NP4	24/240 (1:10)	4000	1400	1400	NP_{50a}
NP5	24/360 (1:15)	4000	1400	1400	NP_{50}
NP6	24/480 (1:20)	4000	1400	1400	NP_{50b}
NP7	24/240 (1:10)	4000	2100	700	NP_{75a}
NP8△	24/360 (1:15)	4000	2100	700	NP_{75}
NP9	24/480 (1:20)	4000	2100	700	NP_{75b}

* indicates the selected NP formulation for in vitro studies

△ indicates the selected NP formulation for in vivo studies.

Table S2. Different *p53*-mRNA sequences used in this study.

Type of *p53*-mRNA	Sequence
Human *p53*-mRNA Open Reading Frame (ORF) sequence	AUGGAGGAGCCGCAGUCAGAUCCUAGCGUCGAGCCCCCU CUGAGUCAGGAAACAUUUUCAGACCUAUGGAAACUACU UCCUGAAAACAACGUUCUGUCCCCCUUGCCGUCCCAAGC AAUGGAUGAUUUGAUGCUGUCCCCGGACGAUAUUGAAC AAUGGUUCACUGAAGACCCAGGUCCAGAUGAAGCUCCCA GAAUGCCAGAGGCUGCUCCCCCCGUGGCCCCUGCACCAG CAGCUCCUACACCGGCGGCCCCUGCACCAGCCCCCUCCU GGCCCCUGUCAUCUUCUGUCCCUUCCCAGAAAACCUACC AGGGCAGCUACGGUUUCCGUCUGGGCUUCUUGCAUUCUG GGACAGCCAAGUCUGUGACUUGCACGUACUCCCCUGCCC UCAACAAGAUGUUUUGCCAACUGGCCAAGACCUGCCCUG UGCAGCUGUGGGUUGAUUCCACACCCCCGCCCGGCACCC GCGUCCGCGCCAUGGCCAUCUACAAGCAGUCACAGCACA UGACGGAGGUUGUGAGGCGCUGCCCCCACCAUGAGCGCU GCUCAGAUAGCGAUGGUCUGGCCCCUCCUCAGCAUCUUA UCCGAGUGGAAGGAAAUUUGCGUGUGGAGUAUUUGGAU GACAGAAACACUUUUCGACAUAGUGUGGUGGUGCCCUA UGAGCCGCCUGAGGUUGGCUCUGACUGUACCACCAUCCA CUACAACUACAUGUGUAACAGUUCCUGCAUGGGCGGCAU GAACCGGAGGCCCAUCCUCACCAUCAUCACACUGGAAGA CUCCAGUGGUAAUCUACUGGGACGGAACAGCUUUGAGG UGCGUGUUUGUGCCUGUCCUGGGAGAGACCGGCGCACAG AGGAAGAGAAUCUCCGCAAGAAAGGGGAGCCUCACCACG AGCUGCCCCCAGGGAGCACUAAGCGAGCACUGCCCAACA ACACCAGCUCCUCUCCCCAGCCAAAGAAGAAACCACUGG AUGGAGAAUAUUUCACCCUUCAGAUCCGUGGGCGUGAG CGCUUCGAGAUGUUCCGAGAGCUGAAUGAGGCCUUGGA

	ACUCAAGGAUGCCCAGGCUGGGAAGGAGCCAGGGGGGA GCAGGGCUCACUCCAGCCACCUGAAGUCCAAAAAGGGUC AGUCUACCUCCCGCCAUAAAAAACUCAUGUUCAAGACAG AAGGGCCUGACUCAGACUGA
Mutant human *p53*-*R175H*-mRNA ORF sequence	AUGGAGGAGCCGCAGUCAGAUCCUAGCGUCGAGCCCCCU CUGAGUCAGGAAACAUUUUCAGACCUAUGGAAACUACU UCCUGAAAACAACGUUCUGUCCCCCUUGCCGUCCCAAGC AAUGGAUGAUUUGAUGCUGUCCCCGGACGAUAUUGAAC AAUGGUUCACUGAAGACCCAGGUCCAGAUGAAGCUCCCA GAAUGCCAGAGGCUGCUCCCCGCGUGGCCCCUGCACCAG CAGCUCCUACACCGGCGGCCCCUGCACCAGCCCCCUCCU GGCCCCUGUCAUCUUCUGUCCCUUCCCAGAAAACCUACC AGGGCAGCUACGGUUUCCGUCUGGGCUUCUUGCAUUCUG GGACAGCCAAGUCUGUGACUUGCACGUACUCCCCUGCCC UCAACAAGAUGUUUUGCCAACUGGCCAAGACCUGCCCUG UGCAGCUGUGGGUUGAUUCCACACCCCCGCCCGGCACCC GCGUCCGCGCCAUGGCCAUCUACAAGCAGUCACAGCACA UGACGGAGGUUGUGAGGCACUGCCCCCACCAUGAGCGCU GCUCAGAUAGCGAUGGUCUGGCCCCUCCUCAGCAUCUUA UCCGAGUGGAAGGAAAUUUGCGUGUGGAGUAUUUGGAU GACAGAAACACUUUUCGACAUAGUGUGGUGGUGCCCUA UGAGCCGCCUGAGGUUGGCUCUGACUGUACCACCAUCCA CUACAACUACAUGUGUAACAGUUCCUGCAUGGGCGGCAU GAACCGGAGGCCCAUCCUCACCAUCAUCACACUGGAAGA CUCCAGUGGUAAUCUACUGGGACGGAACAGCUUUGAGG UGCAUGUUUGUGCCUGUCCUGGGAGAGACCGGCGCACAG AGGAAGAGAAUCUCCGCAAGAAAGGGGAGCCUCACCACG AGCUGCCCCCAGGGAGCACUAAGCGAGCACUGUCCAACA ACACCAGCUCCUCUCCCCAGCCAAAGAAGAAACCACUGG AUGGAGAAUAUUUCACCCUUCAGAUCCGUGGGCGUGAG CGCUUCGAGAUGUUCCGAGAGCUGAAUGAGGCCUUGGA ACUCAAGGAUGCCCAGGCUGGGAAGGAGCCAGGGGGGA GCAGGGCUCACUCCAGCCACCUGAAGUCCAAAAAGGGUC AGUCUACCUCCCGCCAUAAAAAACUCAUGUUCAAGACAG AAGGGCCUGACUCAGACUGA
Murine *p53*-mRNA ORF sequence	AUGACUGCCAUGGAGGAGUCACAGUCGGAUAUCAGCCUC GAGCUCCCUCUGAGCCAGGAGACAUUUUCAGGCUUAUGG AAACUACUUCCUCCAGAAGAUAUCCUGCCAUCACCUCAC UGCAUGGACGAUCUGUUGCUGCCCCAGGAUGUUGAGGA GUUUUUUGAAGGCCCAAGUGAAGCCCUCCGAGUGUCAG GAGCUCCUGCAGCACAGGACCCUGUCACCGAGACCCCUG GGCCAGUGGCCCCUGCCCCAGCCACUCCAUGGCCCCUGU CAUCUUUUGUCCCUUCUCAAAAAACUUACCAGGGCAACU AUGGCUUCCACCUGGGCUUCCUGCAGUCUGGGACAGCCA AGUCUGUUAUGUGCACGUACUCUCCUCCCCUCAAUAAGC UAUUCUGCCAGCUGGCGAAGACGUGCCCUGUGCAGUUGU GGGUCAGCGCCACACCUCCAGCUGGGAGCCGUGUCCGCG CCAUGGCCAUCUACAAGAAGUCACAGCACAUGACGGAGG UCGUGAGACGCUGCCCCCACCAUGAGCGCUGCUCCGAUG GUGAUGGCCUGGCUCCUCCCCAGCAUCUUAUCCGGGUGG

	AAGGAAAUUUGUAUCCCGAGUAUCUGGAAGACAGGCAG ACUUUUCGCCACAGCGUGGUGGUACCUUAUGAGCCACCC GAGGCCGGCUCUGAGUAUACCACCAUCCACUACAAGUAC AUGUGUAAUAGCUCCUGCAUGGGGGGCAUGAACCGCCG ACCUAUCCUUACCAUCAUCACACUGGAAGACUCCAGUGG GAACCUUCUGGGACGGGACAGCUUUGAGGUUCGUGUUU GUGCCUGCCCUGGGAGAGACCGCCGUACAGAAGAAGAAA AUUUCCGCAAAAAGGAAGUCCUUUGCCCUGAACUGCCCC CAGGGAGCGCAAAGAGAGCGCUGCCCACCUGCACAAGCG CCUCUCCCCCCGCAAAAGAAAAAACCACUUGAUGGAGAGU AUUUCACCCUCAAGAUCCGCGGGCGUAAACGCUUCGAGA UGUUCCGGGAGCUGAAUGAGGCCUUAGAGUUAAAGGAU GCCCAUGCUACAGAGGAGUCUGGAGACAGCAGGGCUCAC UCCAGCUACCUGAAGACCAAGAAGGGCCAGUCUACUUCC CGCCAUAAAAAAACAAUGGUCAAGAAAGUGGGGCCUGA CUCAGACUGA

Table S3. Primer sequences for qRT-PCR.

Gene	Primer sequences
GAPDH	Forward: 5’-CCATGGGGAAGGTGAAGGTC-3’ Reverse: 5’-AGTGATGGCATGGACTGTGG-3’
p53	Forward: 5’-ATGGAGGAGCCGCAGTCAGATCCTAG-3’ Reverse: 5’-TCAGTCTGAGTCAGGCCCTTC-3’
ULK1	Forward: 5’-TCCGGATTCGGATTAGCAGC-3’ Reverse: 5’-GGAGAACTCGAACTTGCCCA-3’
ATG7	Forward: 5’-ACCCAG AAGAAGCTGAACGA-3’ Reverse: 5’-CTCATTTGCTGCTTGTTCCA-3’
BECN1	Forward: 5’-GAAGTTTTCCGGCGGCTACC-3’ Reverse: 5’-CTCAGCCCCCGATGCTCTTC-3’
ATG12	Forward: 5’-AAGTGGGCAGTAGAGCGAAC-3’ Reverse: 5’-CACGCCTGAGACTTGCAGTA-3’
TIGAR	Forward: 5’-AAGCAGAGCCTGTCGCTTAG-3’ Reverse: 5’-GCACCACCGCTCTACTGAAT-3’
DRAM1	Forward: 5’-AGTTCGGGGTAGCTCCTCAT-3’ Reverse: 5’-GAGTCGCAGTGAACCCAGAA-3’
ISG20L1	Forward: 5’-CGTGCAGACCGGAAGAGACA-3’ Reverse: 5’-GTGGACATACTTGAGCGCCT-3’
SESN1	Forward: 5’-ACGGATTTGACAGCTCCACA-3’ Reverse: 5’-ACCCATCCGAAGACTCGGTA-3’